Unsaturated Characteristics of Fouled Ballast to Support In Situ Identification of Fouling Using Ground Penetrating Radar – Phase II

REPORT DOCUMENTATION PAGE	*Form Approved* *OMB No. 0704-0188*

The public reporting burden for this collection of information is estimated to average 1 hour per response, including the time for reviewing instructions, searching existing data sources, gathering and maintaining the data needed, and completing and reviewing the collection of information. Send comments regarding this burden estimate or any other aspect of this collection of information, including suggestions for reducing the burden, to Department of Defense, Washington Headquarters Services, Directorate for Information Operations and Reports (0704-0188), 1215 Jefferson Davis Highway, Suite 1204, Arlington, VA 22202-4302. Respondents should be aware that notwithstanding any other provision of law, no person shall be subject to any penalty for failing to comply with a collection of information if it does not display a currently valid OMB control number.
PLEASE DO NOT RETURN YOUR FORM TO THE ABOVE ADDRESS.

1. REPORT DATE *(DD-MM-YYYY)*	2. REPORT TYPE Technical Report	3. DATES COVERED *(From - To)* October 15, 2020–January 15, 2022

4. TITLE AND SUBTITLE Unsaturated Characteristics of Fouled Ballast to Support in Situ Identification of Fouling Using Ground Penetrating Radar – Phase II	5a. CONTRACT NUMBER
	5b. GRANT NUMBER
	5c. PROGRAM ELEMENT NUMBER
6. AUTHOR(S) Stacey E. Kulesza, PhD, PE, 0000-0003-3283-6235 Michelle L. Barry, PhD, PE, 0000-0002-0947-5307 Ruimin Feng PhD, 0000-0001-9184-2702 William Radnor, 0000-0003-0273-545X Debojit Sarker, PhD, 0000-0003-0459-8890 Kyle Parr, 0000-0001-9305-4267	5d. PROJECT NUMBER
	5e. TASK NUMBER
	5f. WORK UNIT NUMBER

7. PERFORMING ORGANIZATION NAME(S) AND ADDRESS(ES) Kansas State University, 1701C Platt St, 2118 Fielder Hall, Manhattan, KS 66506 University of Arkansas, 210 Administration Building, Fayetteville, AR 72701 Texas State University, 601 University Drive, San Marcos, TX 78666	8. PERFORMING ORGANIZATION REPORT NUMBER KSU-UoA-TXST-2022-Phase-II

9. SPONSORING/MONITORING AGENCY NAME(S) AND ADDRESS(ES) U.S. Department of Transportation Federal Railroad Administration Office of Railroad Policy and Development Office of Research, Development, and Technology Washington, DC 20590	10. SPONSOR/MONITOR'S ACRONYM(S)
	11. SPONSOR/MONITOR'S REPORT NUMBER(S) DOT/FRA/ORD-23/18

12. DISTRIBUTION/AVAILABILITY STATEMENT
This document is available to the public through the FRA website.

13. SUPPLEMENTARY NOTES
COR: Hugh Thompson

14. ABSTRACT
The Federal Railroad Administration funded researchers from Kansas State University and the University of Arkansas to establish the electromagnetic, suction, and strength characteristics of fouled ballast as a function of the fouling material and volumetric water content. The team previously established the unsaturated characteristics of various fouling materials and preliminary large scale strength measurements in Phase I. In Phase II, researchers developed a custom electromagnetic sensor. The two research teams conducted experiments from October 2020 through January 2022. They worked with two types of clean ballast and specimens of fouled granitic ballast comprised of various percentages of four fouling materials over a range of volumetric water contents. Ultimately, the team showed the potential for broad spectrum complex impedance measurements to support ground penetrating radar in the field with a full wave form inversion to rapidly identify the type of fouling, degree of fouling, and loss of strength due to fouling.

15. SUBJECT TERMS
Ballast stability detection technology, suction water characteristic curves, large-scale direct shear, complex impedance, ballast fouling, track

16. SECURITY CLASSIFICATION OF:			17. LIMITATION OF ABSTRACT	18. NUMBER OF PAGES	19a. NAME OF RESPONSIBLE PERSON Hugh B. Thompson
a. REPORT	b. ABSTRACT	c. THIS PAGE		63	19b. TELEPHONE NUMBER *(Include area code)* (202) 493-6383

Standard Form 298 (Rev. 8/98)
Prescribed by ANSI Std. Z39.18

i

METRIC/ENGLISH CONVERSION FACTORS

ENGLISH TO METRIC

LENGTH (APPROXIMATE)

1 inch (in)	=	2.5 centimeters (cm)
1 foot (ft)	=	30 centimeters (cm)
1 yard (yd)	=	0.9 meter (m)
1 mile (mi)	=	1.6 kilometers (km)

AREA (APPROXIMATE)

1 square inch (sq in, in^2)	=	6.5 square centimeters (cm^2)
1 square foot (sq ft, ft^2)	=	0.09 square meter (m^2)
1 square yard (sq yd, yd^2)	=	0.8 square meter (m^2)
1 square mile (sq mi, mi^2)	=	2.6 square kilometers (km^2)
1 acre = 0.4 hectare (he)	=	4,000 square meters (m^2)

MASS - WEIGHT (APPROXIMATE)

1 ounce (oz)	=	28 grams (gm)
1 pound (lb)	=	0.45 kilogram (kg)
1 short ton = 2,000 pounds (lb)	=	0.9 tonne (t)

VOLUME (APPROXIMATE)

1 teaspoon (tsp)	=	5 milliliters (ml)
1 tablespoon (tbsp)	=	15 milliliters (ml)
1 fluid ounce (fl oz)	=	30 milliliters (ml)
1 cup (c)	=	0.24 liter (l)
1 pint (pt)	=	0.47 liter (l)
1 quart (qt)	=	0.96 liter (l)
1 gallon (gal)	=	3.8 liters (l)
1 cubic foot (cu ft, ft^3)	=	0.03 cubic meter (m^3)
1 cubic yard (cu yd, yd^3)	=	0.76 cubic meter (m^3)

TEMPERATURE (EXACT)

[(x-32)(5/9)] °F = y °C

METRIC TO ENGLISH

LENGTH (APPROXIMATE)

1 millimeter (mm)	=	0.04 inch (in)
1 centimeter (cm)	=	0.4 inch (in)
1 meter (m)	=	3.3 feet (ft)
1 meter (m)	=	1.1 yards (yd)
1 kilometer (km)	=	0.6 mile (mi)

AREA (APPROXIMATE)

1 square centimeter (cm^2)	=	0.16 square inch (sq in, in^2)
1 square meter (m^2)	=	1.2 square yards (sq yd, yd^2)
1 square kilometer (km^2)	=	0.4 square mile (sq mi, mi^2)
10,000 square meters (m^2)	=	1 hectare (ha) = 2.5 acres

MASS - WEIGHT (APPROXIMATE)

1 gram (gm)	=	0.036 ounce (oz)
1 kilogram (kg)	=	2.2 pounds (lb)
1 tonne (t)	=	1,000 kilograms (kg)
	=	1.1 short tons

VOLUME (APPROXIMATE)

1 milliliter (ml)	=	0.03 fluid ounce (fl oz)
1 liter (l)	=	2.1 pints (pt)
1 liter (l)	=	1.06 quarts (qt)
1 liter (l)	=	0.26 gallon (gal)
1 cubic meter (m^3)	=	36 cubic feet (cu ft, ft^3)
1 cubic meter (m^3)	=	1.3 cubic yards (cu yd, yd^3)

TEMPERATURE (EXACT)

[(9/5) y + 32] °C = x °F

QUICK INCH - CENTIMETER LENGTH CONVERSION

Inches	0	1	2	3	4	5
Centimeters	0 1 2 3 4 5	6 7	8 9 10	11 12 13		

QUICK FAHRENHEIT - CELSIUS TEMPERATURE CONVERSIO

°F	-40°	-22°	-4°	14°	32°	50°	68°	86°	104°	122°	140°	158°	176°	194°	212°
°C	-40°	-30°	-20°	-10°	0°	10°	20°	30°	40°	50°	60°	70°	80°	90°	100°
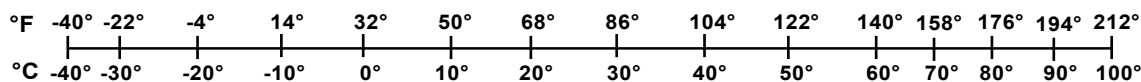
For more exact and or other conversion factors, see NIST Miscellaneous Publication 286, Units of Weights and Measures. Price $2.50 SD Catalog No. C13 10286 **Updated 6/17/98**

Acknowledgements

Contents

Illustrations

Tables

Executive Summary

The Federal Railroad Administration (FRA) funded researchers from Kansas State University and the University of Arkansas to establish the electromagnetic, suction, and strength characteristics of fouled ballast as a function of the fouling material and volumetric water content. The team previously established the unsaturated characteristics of various fouling materials and preliminary large scale strength measurements in Phase I. In Phase II, researchers developed a custom electromagnetic sensor. After transferring to Texas State University (San Marcos, TX), the team continued sensor development and testing by measuring and modeling fouled ballast unsaturated characteristics and complex impedance (i.e., electromagnetic) response. Researchers at the University of Arkansas conducted large-scale direct shear (LSDS) testing on the same materials tested by the Kansas State University/Texas State University team. The two research teams conducted experiments from October 2020 through January 2022. They worked with two types of clean ballast and specimens of fouled granitic ballast comprised of various percentages of four fouling materials over a range of volumetric water contents.

The two teams measured ten specimen suction water characteristic curves (SWCC) and their shear stress and volumetric responses. They mixed clean granitic ballast with each of four fouling materials (i.e., two sands, one coal, and one clay) to different degrees of fouling. Researchers defined the degree of fouling as the relative percentage of fouling material to the dry mass of the ballast; the degree of fouling was 5, 10, and 15 percent to create specimens ranging from moderately clean to fouled. Team members prepared all specimens to a relative density of 85 percent based on clean ballast. They measured the SWCCs in a custom cell validated in Phase I of this research and modeled using a common equation that fits most soil types. The experimental results indicated fouled ballast has a very low residual suction relative to soil. Therefore, the Texas State team used a correction factor that is typically approximated in soils. Results include the experimental data, the model parameters, and fitting statistics for all ten specimens.

Researchers at the University of Arkansas used the SWCC results to guide LSDS specimen preparation and to interpret differences in peak shear stress measurements. They used peak shear stress measurements obtained under a vertical effective stress of 69 kPa (10 psi) as indicators of the fouled ballast specimen strength. In total, the team conducted 52 direct shear tests and found that the peak shear stress decreased with increasing degrees of fouling and volumetric water contents. Researchers determined that out of the four fouling materials tested, the coal fouled specimens resulted in the greatest peak stress reduction with increasing water content. The team was surprised to find that clean basalt ballast also showed a reduction in peak stress with increasing water content, although clean granite ballast did not.

The team at Texas State also developed a prototype circuit board and system for measuring fouling material complex impedance in this study. Researchers validated the prototype with a calibrated system that was ultimately used because it was more efficient after the prototype was damaged. This report contains a summary of the unique experimental setup the team developed for measuring the complex impedance of saturated and unsaturated fouling materials. Previous researchers had primarily tested the complex impedance of saturated core samples. Thus, literature existed on saturated sediments with very little detail on specimen preparation. This study presents the first known results on the complex impedance. The results indicated that there was a clear, strong phase angle response in saturated clay while saturated coal and sand were

near constant phase angle. On the other hand, the three materials were differentiable with unsaturated measurements, which were possible down to an approximately 20 percent degree of saturation with the developed experimental setup.

Researchers sought to combine the three measurements (i.e., SWCC, LDDS, and broad spectrum phase angle) to determine the unsaturated characteristics of fouled ballast. While the volumetric water content was shown to affect the peak shear stress, it alone was not a unique predictor of ballast response. For example, for 10 percent fouling by mass, the coal and clay fouled specimens exhibited similar SWCC responses with similar residual water content, yet the peak stress was significantly lower for the coal fouled specimens. The team found that the clay fouled specimens likely had a higher unsaturated strength compared to the other materials due to interparticle forces and apparent cohesion caused by suction. The clay particles likely lubricated the aggregates as evident by the reduction in strength compared to clean ballast, but this lubrication alone did not significantly reduce the interlocking at ballast-to-ballast contacts. The sand fouled specimen peak shear stress was low due to a lack of suction related interparticle forces and from the sand grains reducing ballast to ballast contacts. Researchers observed that the lowest drop in strength by coal was likely a combination of the clay and sand responses. The coal fouled specimens did have residual water contents similar to the clay, however there was likely a greater volume of coal fouling material and this increase in volume increased the residual water content. This was compounded by the effects of the increase in volume of coal and the presence of sand reducing ballast-to-ballast contacts. Finally, the team determined that at this stage the unsaturated phase angles of the three ballast fouling materials show promise as a qualitative indicator of material type. The differences in the measured complex impedance responses were likely due to differences at particle-to-particle interfaces. These results highlight the potential for using complex impedance to identify different interparticle forces, which likely control the peak shear stress response. Ultimately, the team showed the potential for broad spectrum complex impedance measurements to support ground penetrating radar in the field with a full wave form inversion to rapidly identify the type of fouling, degree of fouling, and loss of strength due to fouling.

1. Introduction

The Federal Railroad Administration (FRA) funded researchers from Kansas State University and the University of Arkansas to establish the electromagnetic, suction, and strength characteristics of fouled ballast as a function of the fouling material and volumetric water content. The team previously established the unsaturated characteristics of various fouling materials and preliminary large scale strength measurements in Phase I. This report includes Phase II results of Kansas State University/Texas State University's fouled ballast suction water characteristic curves (SWCCs), recommendations for unsaturated complex impedance measurements, and complex impedance fouling material results. The results from the University of Arkansas' fouled ballast large-scale direct shear (LSDS) tests are also included. Researchers conducted experiments from October 2020 through January 2021 at Kansas State University in Manhattan, KS, the University of Arkansas in Fayetteville, AR, and Texas State University in San Marcos, TX.

1.1 Background

FRA and the rail industry have recognized the potential of using ground penetrating radar (GPR) for providing real time, automatic mapping of ballast condition to identify the need for remediation [1]. Although extensive research on GPR for identifying fouled ballast exists, the results remain highly affected by moisture, density, parent fouling material, and ballast aggregate mineralogy, making field interpretations difficult. Furthermore, there has been limited research on whether a loss of strength can be identified by electromagnetic properties that influence GPR. There is a need to identify and quantify how in situ ballast conditions affect the strength and stability of the ballast and to what extent those conditions can be identified by electromagnetic properties. In some cases, even a small amount of fouling has been shown to affect the track performance, yet there are other cases of fouled ballast that present no loss of support or show no detectible changes in track geometry despite the reduced drainage capacity. Researchers worked to identify the factors that contribute to ballast strength loss due to fouling and the sensitivity and extent to which they can be measured by complex impedance (i.e., a property that influences GPR [2]).

GPR detects changes in electromagnetic impedance via the transmission and measured reflections of electromagnetic waves. Dielectric constant is the most important parameter in GPR measurements as it determines the wave velocity, reflection coefficients, and attenuation. GPR is a potential tool for nondestructive quantification of undesirable track conditions because fouling, moisture conditions, and density change the ballast's dielectric constant [3]. Although most GPR research focuses on the dielectric constant, this study measured the complex dielectric permittivity (i.e., complex impedance). Complex impedance describes a material's response to an applied electric field providing information of both energy stored and energy lost as

$$\epsilon_T(\omega) = \epsilon_T'(\omega) - i\epsilon_T''(\omega)$$

where the real component, $\epsilon_T'(\omega)$, describes the dielectric polarization and the quadrature component, $i\epsilon_T''(\omega)$, describes the energy lost due to polarization lag, both as a function of frequency (ω). In complex measurements the full response (i.e., in phase and quadrature) is measured with varying frequencies, typically 10 MHz to 2 GHz for GPR. Although the

measurements do not change, the range of frequencies over which a signal is measured can be different – and when measured over different ranges the name of the measurement also changes. For example, spectral induced polarization measurements are typically from 0.1 Hz to 1 kHz. Many researchers study a "broad band" impedance response (i.e., complex impedance). Interfacial polarizations due to the heterogeneous interfaces between particles can be identified with broad bank complex measurements and were of interest in this study.

Typical electromagnetic measurements for ballast have neglected the imaginary component of the complex response for simplification. Alsaban et al. [4] focused on the relative permittivity assuming the imaginary component of the complex measurement to be insignificant and at a limited range of water contents. Sussmann et al. [5] similarly measured the relative permittivity of fouled ballast in the laboratory as a reference for interpreting GPR results of fouled ballast in the field. The limited research into the complex electromagnetic properties of ballast is likely because of previous limitations in data processing and inversion. These complex measurements were originally believed to overcomplicate analyses, but they provide additional data regarding material properties. Geophysical inversions are beginning to leverage these types of full geophysical signatures to improve material characterization with high resolution methods [6]. Because existing studies on fouled ballast were in the higher GPR range, this research focused on the 0.1 to 20 kHz range and contributed new data. Understanding the complex parameters of dielectric permittivity has been established as a critical issue for physical interpretation of material composition when using GPR. By measuring the complex impedance, more information is collected for full wave form inversion which considers the full frequency-domain signature of measured data for improved resolution and material identification [7]. This is a critical step needed for quantitatively considering GPR for fouled ballast.

In Phase I of this study, researchers established the SWCCs of 17 samples of fouling materials collected from various track locations across the U.S. [8, 9]. The SWCC is the relationship between water content (i.e., gravimetric or volumetric) or degree of saturation with suction (i.e., matric suction or total) [10]. The net normal stress and matric suction are the factors that define the stress state of an unsaturated soil. The difference between the air and water pressure is referred to as matric suction. The team tested only the fouling materials (i.e., materials passing the No 3/8 sieve) in Phase I to isolate the importance of the fouling material and to develop a protocol for measuring the SWCCs including the ballast aggregate. Researchers found that the fouling material itself greatly impacts the SWCC. Figure 1 shows the SWCCs for a subset of the samples tested in Phase I. In general, the residual water contents of the coarser-grained sand fouling materials (i.e., SP, SW, SM) were quite low, as expected. The silt fouled sample (ML) had a greater residual water content compared to the three sands. The most interesting findings related to two notably different SWCCs for samples that were collected from areas known to be fouled by coal. The first clay sample with coal (i.e., CL1) had 8.5 percent coal content whereas the second clay sample with coal (i.e., CL2) had a coal content of 15 percent. Note that the higher coal content also had higher air entry and higher residual water content. Other samples tested with coal also exhibited a similar variability despite classifying the same geotechnically (i.e., as CL according to the Unified Soil Classification System). Phase I marked the first time that the unsaturated characteristics of fouling materials were measured in this way, and it provided a means of differentiating the unique features of fouling materials that otherwise would traditionally appear similar.
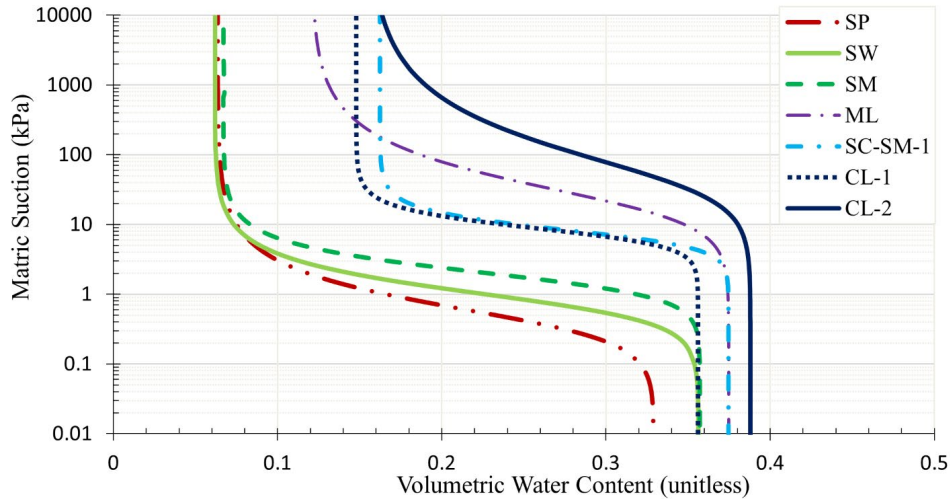
Figure 1: SWCCs of seven fouling materials tested in Phase I

A challenge in working with ballast is the size of the aggregates, which are too large for traditional geotechnical equipment. Therefore, researchers in Phase I established a methodology for measuring fouled ballast SWCCs and validating the custom equipment. The SWCC results of ten fouled ballast specimens tested as a part of this Phase II research are presented in this report. This study highlights how the parent fouling material highly influences the range from saturated to residual water content, even when ballast aggregates are included. This finding also has further implications for the electromagnetic and strength characteristics of fouled ballast. Phase I also included LSDS experimental design to link the SWCC observations with the corresponding shear stress and volumetric behavior during shearing. Initially, the team tested clean dry ballast to obtain the Mohr-Coulomb strength parameters and define the failure envelope. However, significant particle breakage was observed at the higher vertical stresses tested. Therefore, the team selected testing at one stress level to describe the influence of fouling and moisture on ballast response and ensure that replicate tests were at the same gradation. Researchers also performed replicate tests on clean dry and surface wet ballast to determine the variability and repeatability and used preliminary LSDS tests on ballast with 5 percent clay fouling to further guide the testing methods used. Overall, the team in Phase I developed a testing protocol for ensuring replicate samples were prepared in an LSDS device which was guided by the SWCC findings. Researchers used this protocol to obtain LSDS results for the ten fouled ballast specimens as a part of Phase II and presented a comparison of clean granite and basalt ballast. Developing an understanding of the sensitivity of stress and volumetric behavior to the changing fouling conditions is critical in linking the GPR measurements with field performance.

The long-term goal of this research is to be able to use GPR to quantify undesirable track conditions (e.g., loss of strength, percent fouling, changes in void ratio, moisture) regardless of the in-situ ballast and fouling materials. The electromagnetic wave propagation used in GPR is largely controlled by variations in the dielectric permittivity of a medium. Dielectric permittivity is greatly influenced by moisture because molecular polarization of water molecules influences the electromagnetic wave propagation. Researchers in Phase II developed instrumentation to measure the complex impedance (i.e., complex dielectric permittivity) of different fouling

materials at target volumetric water contents. Traditional complex impedance measurements are obtained on fully saturated specimens, mainly intact rock core specimens. Therefore, in Phase II the team developed the experimental device and protocol for testing unsaturated fouling material specimens. This report also contains the complex impedance results of the three fouling materials (i.e., sand, coal, and clay specimens) at two volumetric water contents. Thus, by preparing LSDS and complex impedance specimens as target volumetric water contents guided by the unique SWCC measurements, this study includes qualitative explanations for loss of shear stress in fouled ballast specimens that cannot be explained with traditional geotechnical approaches. As this research continues, it is anticipated that the complex measurements will highlight additional influences of ballast properties on permittivity that ultimately influence GPR.

1.2 Objectives

The objective of this research was to establish the electromagnetic, suction, and strength characteristics of fouled ballast as a function of the fouling material and moisture content. This will improve the fundamental understanding of ballast degradation characteristics, non-destructive identification of fouled ballast in the field, and ultimately improve the performance and safety of the track structure.

1.3 Overall Approach

The research team developed custom equipment and methods to measure the unsaturated characteristics, electromagnetic response, and peak shear stress of fouled ballast specimens. The team used a classic SWCC model and a novel curve fitting approach to model the unsaturated data. They used the SWCC results to guide specimen preparation for the LSDS and ran 52 tests. Team members measured complex impedance on the fouling materials using a custom cell and device. Researchers then combined the three results to explore relationships between loss of peak shear strength due to fouling and moisture considering the unsaturated electromagnetic response.

A quarry in Oklahoma that serves as a major ballast source in the region between Texas and Kansas donated clean granitic ballast. A quarry in Missouri which represents a prominent trap rock source in the region donated additional basalt ballast. Three of the four fouling materials examined in this study were sampled from track in the Midwest, and one was a purchased manufactured clay. The team prepared specimens by compacting ballast to the same target density in each laboratory and adding target percent fouling material by mass (5, 10, and 15 percent). Researchers created 10 specimens for SWCC testing using a custom device developed in Phase I of this research. The team also tested 10 specimens with the LSDS device using the protocol developed in Phase I for measuring the shear stress and volumetric response at target volumetric water contents. They also tested clean granite and basalt ballast specimens to provide a baseline for the fouled ballast specimens and to compare the two ballast sources and mineralogies. The team conducted complex impedance measurements of the four fouling materials at full saturation and target volumetric water contents.

The research team worked to determine the sensitivity of peak shear stress and volumetric response to changing fouling conditions (i.e., fouling material, degree of fouling, and moisture) and identify to what extent that strength loss can be qualitatively described by the fouling material complex impedance response as a function of moisture. This report provides a summary of the Phase II results and how the overarching research questions were answered through the results.

1.4 Scope

This report includes 10 SWCC tests on fouled ballast specimens, 7 LSDS tests on clean ballast, and 45 LSDS tests on fouled ballast with various moisture conditions. Seven complex impedance results on sand fouling as a function of saturation as well as six complex impedance measurements on the three fouling materials as a function of moisture are included. Additional complex impedance experimental results that guided the testing protocol are included in the Appendices. The team primarily focused on one type of ballast but also tested an additional ballast specimen in the LSDS device for comparison. The study likely does not include all fouling materials.

1.5 Organization of the Report

Section 1 contains the introduction, a summary of Phase I, and a literature review. Section 2 describes the research methodology. Section 3 includes results and discussion. Section 4 provides the Phase II conclusions and the overall study conclusions. Additional SWCC experiments not included for clarity are included in Appendix A. Plots of the LSDS tests results are presented in Appendix B and include shear stress versus horizontal displacement and vertical versus horizontal displacement curves. A summary table of the complex impedance design of experiments and all experimental design results are included in Appendix C.

2. Methods

BNSF Railway, Martin Marietta, Inc., and New Frontier Materials donated materials for this project. In Phase I, researchers developed the testing protocol for ensuring replicate samples could be made between the two university labs. The team also developed a custom SWCC device and testing protocol for the LSDS tests in Phase I to ensure percent fouling, density, and water content matched those of the fouled ballast SWCC tests. This report includes the Phase II final results for fouled ballast SWCCs and LSDS tests, along with complex impedance measurements.

2.1 Materials

BNSF donated fresh ballast and three of the four fouling materials tested. The fresh granite ballast was taken from a quarry in Oklahoma and three of the fouling materials were taken from mainline track. All fouling material gradations tested can be seen in Figure 2. Sand 1 and Sand 2 were taken from highly fouled track and washed of all fines that pass the #200 sieve. The specific locations of Sand 1 and Sand 2 were not provided. The fouling material noted as Coal was taken from a track used to transport coal freight. The fourth fouling material, noted as Clay, was purchased from a clay supply company. The material is dry in powder form and packaged in 22.7 kg bags. The Unified Soil Classification System (USCS) group classifications for each of the fouling materials presented in Figure 2 were determined to be: Low plasticity silt, ML (i.e., Coal), Poorly graded sand, SP (i.e., Sand 1 and Sand 2), and Low plasticity clay, CL (i.e., Clay).

Figure 2: Grain size distribution of fouling material used in SWCC and LSDS testing in Phase II

Researchers processed the fresh granite ballast samples to obtain the "as delivered" particle size distribution according to ASTM C136 [11]. Figure 3, Figure 4, and Figure 5 show the particle size distribution of the clean ballast, the upper and lower bound limits corresponding to the Class 1 specified gradations [12], and the gradations under each of the fouling conditions examined. The gradation for clean granite ballast was within the Class 1 boundaries, however, all the fouling conditions tested resulted in distributions which were outside of the upper bound. Note that the basalt gradation shown in Figure 5 was just at or slightly below the lower bound but likely still acceptable in terms of specifications for use. Although studies have shown abraded

ballast to have differing strength properties, the team determined that starting with fresh ballast for each set of tests for different fouling materials and percentages was the best way to ensure comparable results among fouling conditions and among the two research groups. Researchers determined the minimum and maximum densities of the clean granite ballast according to ASTM D4254 [13] and D4253 [14] to be 12.92 kN/m^3 and 15.17 kN/m^3, respectively. Each test targeted a relative density of the ballast of 85 percent and the actual density varied based on the fouling material percentage tested.

Because ballast breakdown is a major source of fouling [15], the team focused the initial testing on sand fouling. The range of particle sizes comprising sand fouling can also vary widely and the sensitivity of the suction, strength, and deformation response for different gradations was of interest. To explore this sensitivity, researchers used two different gradations of sand (i.e., Sand 1 and Sand 2) as the fouling material. Both classified as poorly graded sand, SP, according to the USCS, although they were visually very different in terms of particle size. The fouling materials were obtained and separated from ballast taken from in service track. The team conducted tests at different fouling conditions, where they considered the percent fouling to be the mass of fouling material divided by the total dry weight of the ballast specimen. This approach allowed the two laboratories to focus on specimen preparation via the relative density of the ballast, which researchers determined to be the most consistent method for making replicate samples [8]. Figure 3 shows the gradations of Sand 1 and Sand 2, as well as the gradations of the fouled ballast with 5, 10, and 15 percent fouling materials by weight.
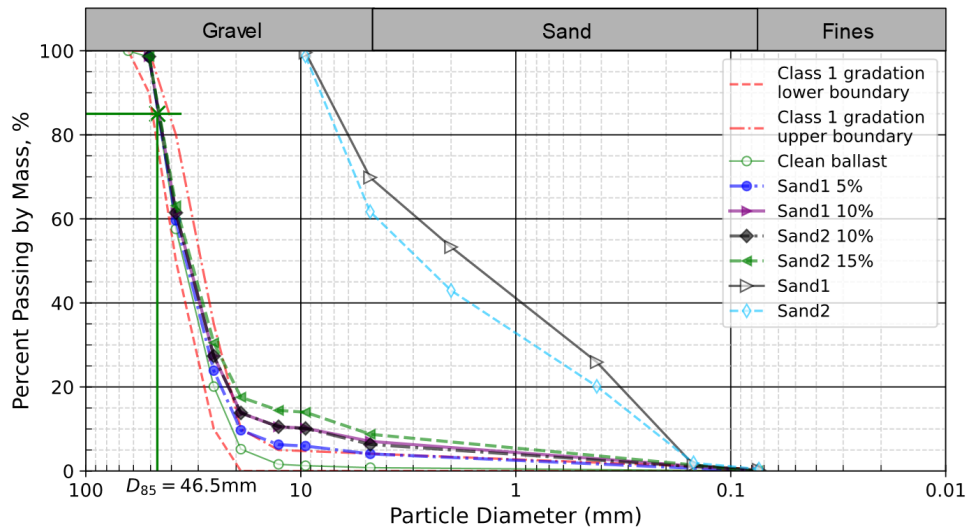
Figure 3: Particle size distribution of clean granite ballast, two types of sand fouling, and fouled ballast samples used in testing

In addition to sand fouling from breakdown of the ballast particles, clay is commonly washed into the ballast during inundation from flooding or pumped in from the subgrade, and coal dust can also infiltrate from the surface. Therefore, the team investigated the influence of different fouling material types on strength and deformation behavior of the ballast. Like the sand fouled ballast, researchers were also interested in examining the sensitivity of the suction, strength, and deformation response for different fouling contents. Figure 4 shows the gradations of clay (CL) and coal (ML) fouled ballast with 5, 10, and 15 percent fouling by weight. Due to the shortage of

coal fouling materials, the team performed LSDS tests only on the ballast with 5 and 10 percent coal fouling.
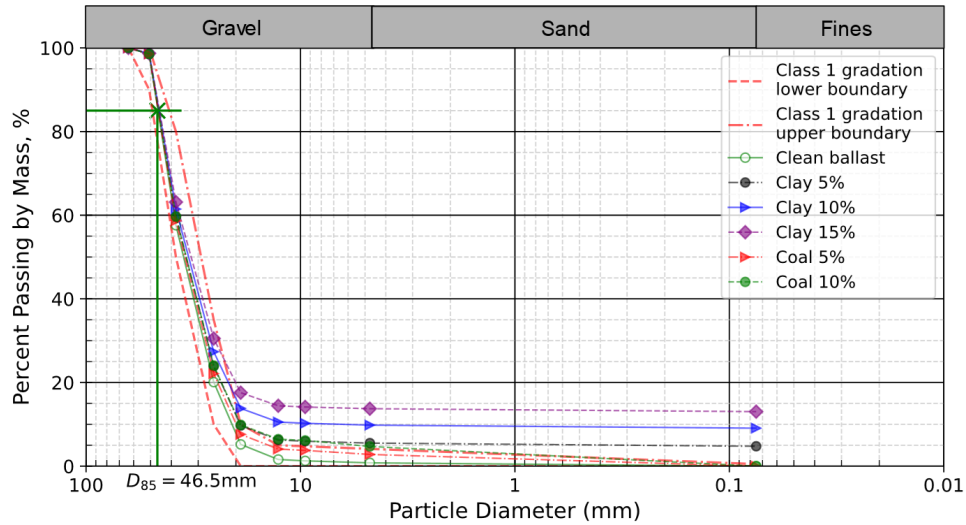
Figure 4: Particle size distribution of clean granite ballast, coal, and clay fouled ballast specimens used in testing

For comparison, the team obtained clean basalt ballast (i.e., trap rock) from a quarry and tested it under the same experimental conditions as the clean granite ballast. The minimum and maximum densities of the clean basalt ballast were 13.77 kN/m^3 and 14.46 kN/m^3. The gradation of the two ballast samples is shown in Figure 5.
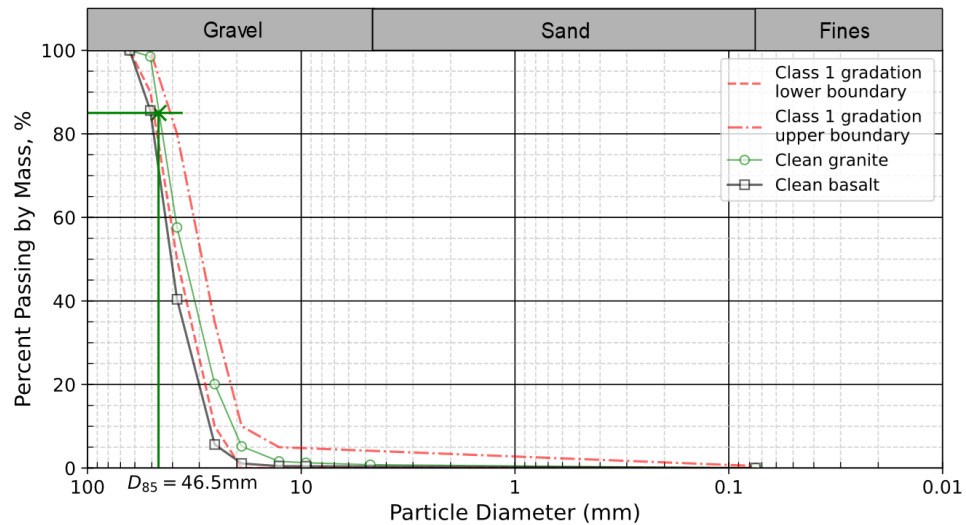
Figure 5: Particle size distribution of clean granite and basalt

Researchers prepared the fouled ballast specimens by mixing clean granite ballast with various degrees of fouling using the four fouling materials. The team regulated the ballast fouling conditions by controlling the percent mass from the fouling materials passing the No. 3/8" sieve, noted as percent fouling. The clean ballast adhered to Class 1 gradation specifications (see Figure 5). The team defined the degree of fouling as the mass of fouling material relative to the mass of the clean ballast to ensure replicate samples could be made between the two laboratories.

Researchers prepared clay fouling specimens to 5, 10, and 15 percent. The Sand 1 specimens were prepared to 5 and 10 percent. The Sand 2 specimen is a mixture of Sand 1 and another sand fouling sample with a similar gradation. Mixing the two gradations resulted in a different gradation than the original Sand 1 (see Figure 2). The team prepared the mixture to have enough material for 15 percent sand fouling in the LSDS testing and then tested 10 and 15 percent specimens with Sand 2. The 5 percent was not tested because the unsaturated results from Sand 1 were difficult to obtain due to the very small amount of fouling material and the differences in terms of peak shear stress were expected to be minimal. The team prepared the coal fouling to 5 and 10 percent. Unfortunately, researchers were not able to obtain enough coal fouling material to achieve 15 percent degree of fouling in the LSDS. Therefore, the team prepared a total of nine specimens.

Researchers characterized all specimens according to the Selig Fouling index (FI)

$$FI = P_4 + P_{200}$$

where P_4 is the percent mass passing the No. 4 sieve (4.75 mm) and P_{200} is the percent mass passing the No. 200 sieve (0.075 mm) [15]. Table 1 shows all specimens and how the degree of fouling compares to the FI as well as the void contamination index (VCI [16]) and relative ballast fouling ratio (RBF [17]) to provide additional metrics that have been used in the literature to classify fouled ballast. The VCI is

$$VCI = \frac{1 + e_f}{e_b} \cdot \frac{G_{sb}}{G_{sf}} \cdot \frac{M_f}{M_b}$$

where e_f is the void ratio of the fouling material, e_b is the void ratio of the ballast aggregate, G_{sf} is the specific gravity of the fouling material, G_{sb} is the specific gravity of the clean ballast, M_b is the dry mass of the clean ballast, and M_f is the dry mass of the fouling material. The relative ballast fouling ratio, R_{b-f} is

$$R_{b-f} = \frac{M_f \left(\frac{G_{b-f}}{G_{s-f}} \right)}{M_b} x100\%$$

where M_f is the dry mass of the fouling, M_b is the dry mass of the ballast, G_{b-f} is the specific gravity of the ballast, and G_{s-f} is the specific gravity of the fouling material. The team classified the laboratory specimens as clean to fouled, depending on the method.

Table 1: Specimen degree of fouling and corresponding fouling category using Selig's Fouling Index, Void Contamination Index, and Relative Ballast Fouling Ratio for laboratory prepared specimens

	Sand 1		Sand 2		Coal		Clay		
Degree of fouling (%)	5	10	10	15	5	10	5	10	15
FI	3.73	7.07	6.33	8.22	7.36	13.3	11.1	19.7	27.4
FI Category	MC	MC	MC	MC	MC	MF	MF	MF	F
VCI (%)	10.9	21.9	21.7	31.2	11.1	22.2	11.0	22.1	33.4
VCI Category	C	MF	MF	F	C	MF	C	MF	F
RBF (%)	6.4	11.5	11.4	15.8	6.60	11.9	6.10	10.9	15.7
RBF Category	MC	MF	MF	MF	MC	MF	MC	MF	MF
FI = Selig Fouling Index; VCI = Void Contamination Index; RBF = Relative Ballast Fouling Ratio. C = Clean; MC = Moderately Clean; MF = Moderately Fouled; F=Fouled									

2.2 SWCC Testing and Modeling

The team used the transient water release and imbibition method (TRIM) system developed by Wayllace & Lu [18] to measure the volumetric moisture content and corresponding matric suction for the SWCCs. The TRIM system is a laboratory setup consisting of a control panel, a flow cell, a high air entry (HAE) ceramic disc, and a scale. Figure 6a shows a schematic of the flow cell; Figure 6b shows the full system. The control panel regulates the amount of pressure or vacuum applied at any given time and the flow cell contains the HAE disc and the soil sample. The HAE disc uses the principal of axis translation in which the HAE disc maintains a steady pressure on top of the disc while on the other side of the disc a steady pore water pressure is maintained at atmospheric conditions [19]. A scale is used to measure how much water is imbibed into the specimen under vacuum and how much water is expelled under pressure.
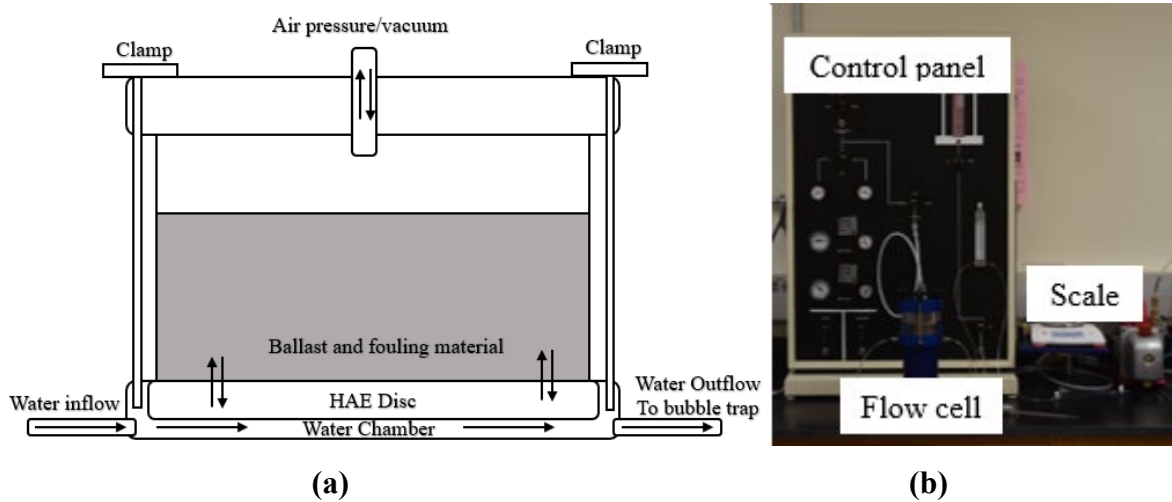

(a)   (b)

Figure 6: Custom TRIM: (a) Flow cell schematic; (b) experimental setup

The team measured the SWCCs of fouling materials in Phase I with a standard TRIM flow cell (height of 66 mm and diameter of 61 mm) [18]. Due to the large nature of ballast (i.e., 38.1 mm in length that varies with thickness and width), Phase I researchers developed a large flow cell with a height of 17.8 cm and a diameter of 25.5 cm [8]. The team modified the standard TRIM procedure to allow for additional measurements so they could explore additional SWCC models more appropriate for ballast. The standard TRIM test simultaneously measures the hydraulic conductivity function and uses the van Genuchten model [20] to solve an inverse problem with only two direct measurements of suction; however, this method was not effective for fouled ballast because it was difficult to obtain the hydraulic conductivity function of the specimens.

The coefficient of water volume change with respect to matric suction is given by the slope of the SWCC. Over the years, several researchers proposed a number of equations for the SWCC. Among various forms of equations suggested by different researchers, Leong and Rahardjo [21] showed that Fredlund and Xing's [22] equation performs very well for all soil types, so the team considered it for estimating the SWCCs of fouled ballast. The experimental results indicate that the residual suction for fouled ballast is relatively small compared to other soil types. For this reason, a correction is needed to accurately predict the mathematical shape of SWCCs from the measured dataset obtained from the tests. Fredlund and Xing [22] presented a correction factor that eliminates the requirement for the residual water content as fitting parameter and reduces the complexity of the model. However, the correction is dependent on the value selected for the residual suction; in general, it is possible to use a value of 1500 kPa as an approximation for most soils. The Fredlund and Xing [22] correction is a logarithmic equation followed by mathematical consideration that is unity in the wet zone and zero water content at 10^6 kPa.

2.2.1 Specimen Preparation

Researchers prepared a 7.1±.1 kg clean ballast sample following the "as delivered" granite gradation (Figure 5). The amount of fouling combined with the ballast was based on a percentage of the total clean ballast. The team separated the gradation and ballast into three lifts, placing the ballast in each lift and combining it with the fouling material. Each lift had a target height of 3.2 cm per lift. The team measured each lift from the top of the cell to the top of the ballast. Lifts were placed within ± 2 mm of the target height to obtain a relative density of 85 percent ± 2 percent. Researchers recorded nine measurements for each lift and produced an average. A target 85 percent relative density was used because it was the maximum relative density that could be achieved during SWCC testing without breaking the large ceramic disc at the bottom of the flow cell [8].

2.2.2 Testing Procedure

Researchers used two HAE ceramic discs in the TRIM: a 0.5-bar (~ 50 kPa) high-flow disc and a 1-bar (~ 100 kPa) disc. Saturation of the HAE disc was confirmed by mass. The approximate amount of water needed to fill the voids in the ballast to achieve full saturation was determined based on ballast porosity. Water was imbibed via vacuum through the HAE disc and tracked with a scale. The team compared the total water imbibed with the theoretical amount needed and was found to be within ±10g for each test. At the end of imbibition, water was allowed to freely outflow and was tracked via logging software. Some water was still retained on top of the stone that was not necessarily retained by the fouling material due to negative porewater pressure in the stone. This was apparent because of a visible layer of water on top of the HAE disc that

would have otherwise drained freely. Thus, the first pressure step of 0.4 kPa was used to expel the remaining water ponded on the stone. This was the lowest pressure that could be maintained consistently with the pressure regulator.

Next the team slowly increased the pressure until water began to outflow from the fouling material, typically 0.6 kPa. Eight increasing pressure increments were obtained. For the 0.5-bar stone, the final pressure was 30 kPa. For the 1-bar stone, the final pressure was 80 kPa. The multiple pressure steps allowed for measuring the decrease in volumetric moisture content with the corresponding matric suction. Researchers verified the volumetric moisture contents recoded by the large flow cell through two clay fouling tests. The first test was to measure different matric suctions and volumetric moisture contents from 0.4-80 kPa. The second was taken to one pressure step 30 kPa, where a gravimetric water content was obtained and converted to volumetric moisture content. The two tests had a difference of ±1.5 percent of the calculated volumetric moisture content. The verification results are included in Appendix A. After the final pressure increment the team removed the specimen from the cell and oven dried it to find the final gravimetric water content. In addition, a sub sample of the fouling material was also taken to measure the final gravimetric water content of the fouling material.

2.2.3 Modeling

Researchers plotted the nine measured volumetric moisture contents and their respective suction and fit them with a classic SWCC model. The full saturation point was assumed to occur at 0.001 kPa. Due to the limitations of the control panel pressure regulator, measurements below 0.4 kPa were not possible. The team calculated a low moisture content measurement near air entry for all samples using Li et al. [23], which calculates SWCC data based on gradation. This gradation-based measurement is shown with an open circle on all models and was validated based on the goodness of fit parameters for the four-parameter model. The team fitted all the SWCCs following the Fredlund and Xing [22] equation with a correction factor, $C(\Psi)$

$$\theta(\Psi) = C(\Psi) * \frac{\theta_s}{\left\{ ln\left[e + \left(\frac{\Psi}{a} \right)^n \right] \right\}^m}$$

where θ is the volumetric moisture content, a, n, m are the fitting parameters, θ_s is the saturated volumetric moisture content, and ψ is the suction. The Fredlund and Xing [22] correction factor is

$$C(\Psi) = \left[1 - \frac{ln\left(1 + \frac{\Psi}{C_r} \right)}{ln\left(1 + \frac{10^6}{C_r} \right)} \right]$$

where C_r is the parameter related to the residual suction and the remaining variables have previously been defined. Researchers used a non-linear least squares method to calculate best-fit parameters (e.g., a, n, and m) by best-fitting each data set acquired from SWCC tests. They developed an in-house MATLAB-based software to determine the best-fitting Fredlund and Xing [22] SWCC curve from the dataset obtained through the laboratory experiment [24]. Since the

14

Trust-region method is a widely used numerical method for solving nonlinear programming problems, the team implemented this algorithm into the developed program to determine the fitting parameters. This is done by first defining a region surrounding the current best solution within which a particular model, in this case the Fredlund and Xing [22] equation, can approximate the original objective function. The team obtained all fitting parameters with 95 percent confidence bounds by running the software. It is worth noting that the obtained sum of squared error (SSE) and the square root of the variance of the residuals were extremely low, indicating that the measured data were well fitted.

2.3   Large-scale direct shear testing

Previous studies on ballast strength have focused on LSDS testing [25, 26] and triaxial shear testing [27, 28]. LSDS testing has several advantages, in that tests are simple to conduct and analyze and most importantly it allows for the rotation of the principal planes, which is a key characteristic of field loading conditions. Therefore, researchers performed LSDS tests following the procedures and guidelines specified in ASTM D3080 [29]. Figure 7 shows the custom LSDS apparatus capable of testing 600 mm diameter by 300 mm tall specimens at vertical stress up to 700 kPa. The dimensions satisfy the ASTM D3080 particle to specimen size requirements for the materials examined in this study.
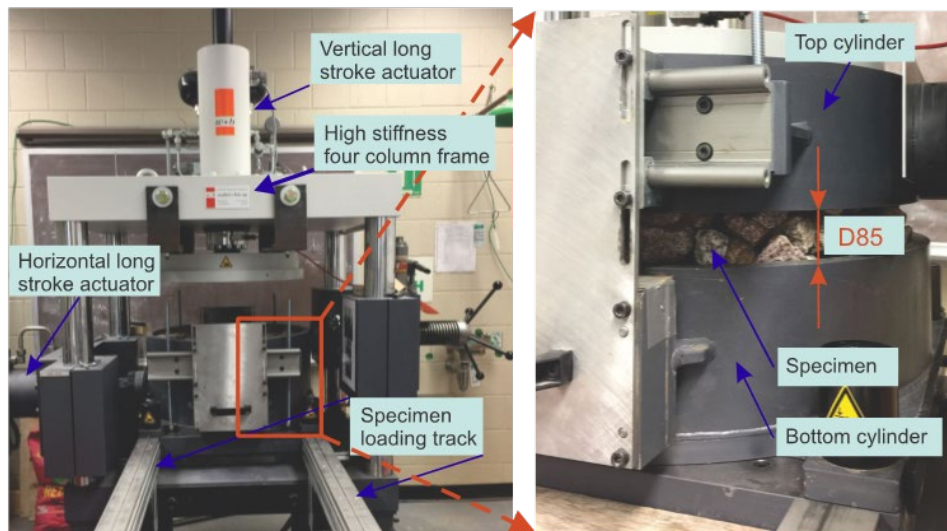

Figure 7: LSDS device with its main components labeled along with the gap sized used during testing

2.3.1   Specimen Preparation

To eliminate any unwanted changes in ballast angularity and gradation, the team obtained a new ballast gradation for every series of LSDS tests. To ensure a uniform density of 85 percent across the specimen, team members placed the ballast into the shear cell and compacted in three lifts to a target final height (checked at a vertical stress of 10 kPa). Meanwhile, as shown in Figure 8, researchers took photographs at the top of each lift and digitally analyzed them to ensure consistent surface porosity (i.e., a 2D estimate of surface area of voids to total surface area) throughout the specimen. Note that the consistency in the value obtained was deemed important and not necessarily the value itself. The team also graded the fouling material and evenly

separated it into three portions, mixing each portion with two buckets of aggregates using a cement mixer and bringing them to the specified water content based on the "free drain" SWCC. In Phase I, the team determined that samples should be prepared in the LSDS at the field capacity or free drained volumetric water content and allowed to air dry to the residual water content, while running tests at the points in between. This allowed for comparisons of strength and volumetric behavior measurements at volumetric water contents measured with the SWCC device. After the first free drain condition test, researchers allowed the specimens to air dry, remixed them to ensure a uniform moisture condition, and compacted them. To measure gravimetric water content, the team collected a reduced portion of the specimen (i.e., a representative mix of ballast and fouling material) along with a small portion containing only the fouling material. This method was determined to be reasonable and rather accurate during the Phase I study. Researchers replicated these tests at both laboratories to ensure repeatable and consistent conditions.
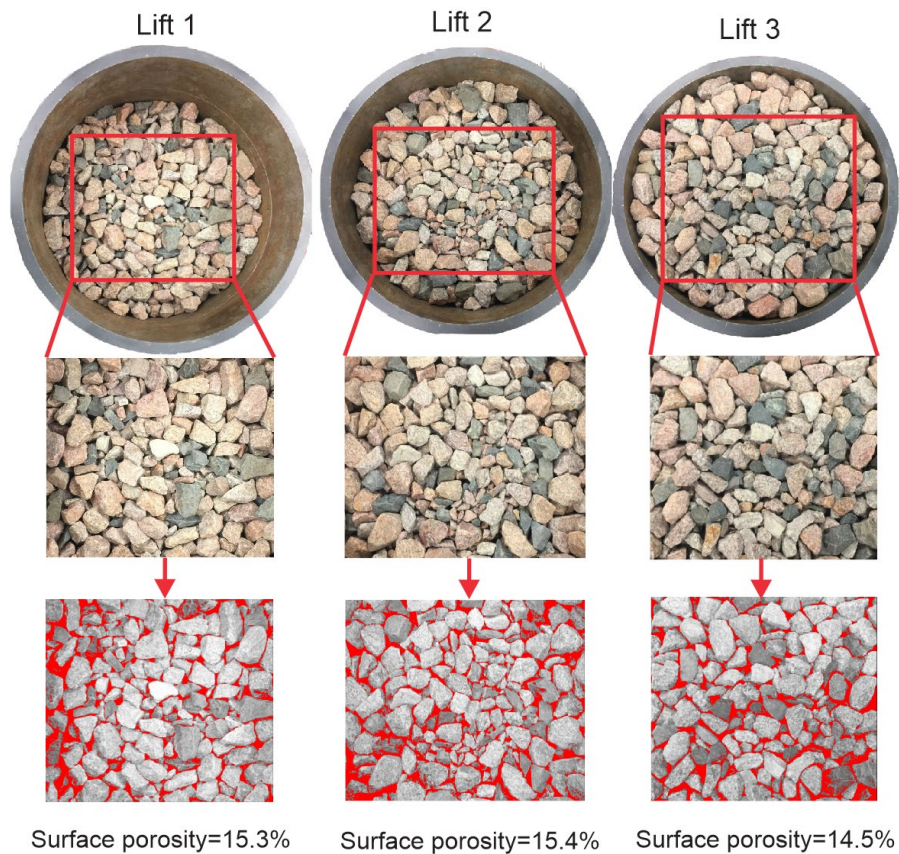

Figure 8: Real-time surface porosity measurements used to ensure a uniform compacted specimen in the LSDS testing

2.3.2 Testing Procedure

After loading the sample into the shear cell and applying the consolidation load, researchers raised the top cylinder vertically using a hanging system to create a gap between the top and bottom cylinder to facilitate proper shearing through the central zone and not overestimate strength. The gap spacing was equal to $D85$ (i.e., the diameter at which 85 percent of the particles by mass are smaller) or 46.5 mm for the granite ballast (Figure 5). The $D85$ was chosen

based on previous experience in aggregate testing and guidance from the Federal Highway Administration for large-scale aggregate testing. Once the gap was set, team members applied the target vertical stress and the sample was sheared at 0.381 mm/min to a horizontal displacement of 135 mm. The shear rate in the standard direct shear test ranged from 5 mm/min to about 0.0003 mm/min [30]. The slow shear rate was used to maintain drained conditions and avoid any buildup of pore water pressure in the specimen voids during shearing. Researchers removed the specimen from the shear cell, allowed it to air dry for 12 hours to reduce the moisture content, and then mixed it using the cement mixer. After measuring the specimen for moisture content, the team re-mixed it and compacted it in three equal lifts for the next test. Tests were conducted until the sample was air dry.

The team initially conducted four LSDS tests (i.e., two dry and two free drain) on clean ballast to: 1) provide a baseline for stress and deformation response comparisons; 2) determine the spectrum of the peak shear stress between the dry and free drain conditions; and 3) assess repeatability and variability among replicate tests. After completing the replicate tests on clean ballast, researchers applied the same experimental procedure for all the following LSDS tests on fouled ballast as shown in the flow chart in Figure 9. The vertical effective stress applied on the sample was maintained at 69 kPa for all tests. This stress level reduced the occurrence of ballast breakdown; by keeping a constant vertical stress, the team was able to understand the role of fouling and moisture in ballast strength and compare it from test to test without having to consider the full range of vertical stresses which would require a large number of tests.
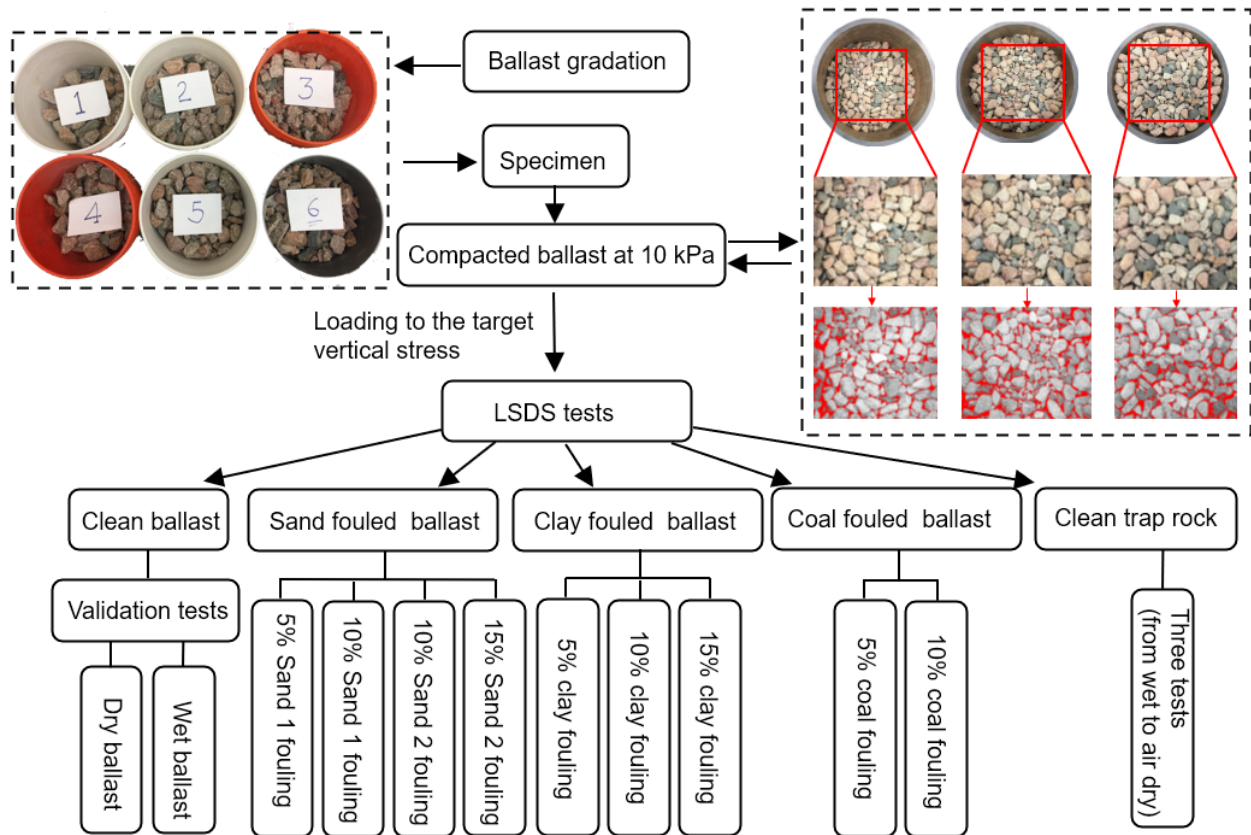

Figure 9: Flow chart of the LSDS tests

17

2.4. Complex impedance testing

The polarization mechanisms that control single component materials (i.e., clean ballast) in the GPR frequency range include electronic, atomic, and molecular polarization [31]. In clean ballast the real component (often reported as relative permittivity) will control the response, primarily due to the molecular polarization of water. However, other polarization mechanisms can be observed at lower frequencies. Researchers used a broad band impedance measurement, from 0.1 to 20 kHz to explore non-molecular polarization effects. The team hypothesized that interfacial charges build up at dissimilar electric properties (i.e., Maxwell-Wagner polarization at high frequencies) and diffusion-driven decays of ionic concentration gradients (i.e., Stern layer polarization and membrane polarization at lower frequencies) would identify interparticle interactions noted in peak shear stress measurements. The team designed a sample holder that can accurately measure the broad band (i.e., 10^{-3} Hz to 10^{11} Hz) response of fouled ballast, including aggregates. The relatively large size of the aggregate and the experimental design related to testing unsaturated materials required a novel specimen holder.

Complex impedance measurements of low polarizability sediments, such as breakdown ballast, are not common. Furthermore, most studies on sediments are on fully saturated specimens. This research is the first to measure the complex impedance of unsaturated ballast fouling materials. Researchers designed a non-conducting acrylic sample holder following recommendations from Zimmerman et al. [32] to reduce phase errors in sediments with low polarizability using a four-electrode configuration. The sample holder was 12 x 12 x 36 cm^3. Because there was limited information regarding unsaturated sediment complex impedance, the team evaluated different current electrode materials (i.e., copper, stainless steel, and copper foam). Potential electrodes included pellet electrodes, silver wire in solution, and McMiller Cu-CuSO4 field electrodes (RE-5 and RE-375). Although the team developed a custom board as designed by Zimmerman et al. [32] for this project, results shown herein used a Gamry Potentiostat because the board was damaged during this study.

2.4.1   Specimen Preparation

Researchers prepared all samples to a target dry density so that the amount of water required to obtain the target volumetric moisture content could be determined and so that specimens could be compared to each other without the influence of a changing pore space. The team thoroughly mixed specimens with the required amount of water, stored them in sealed bags, and allowed them to equilibrate in a 100 percent humidity room for at least 24 hours. First the current electrodes were placed at the edge of the box as shown in Figure 10. The specimens were carefully tamped in the acrylic specimen holder in three equal lifts to achieve the target densities and saturations. All measurements were verified by total mass in the box prior to testing and a calculated water content of the total sample; final dry density and saturation were determined used phase relationships. Potential electrodes were placed flush with the top of the specimen outside the flow of current using burette holders. Having potential electrodes in the current flow can cause a spurious charge and phase measurement errors [33].
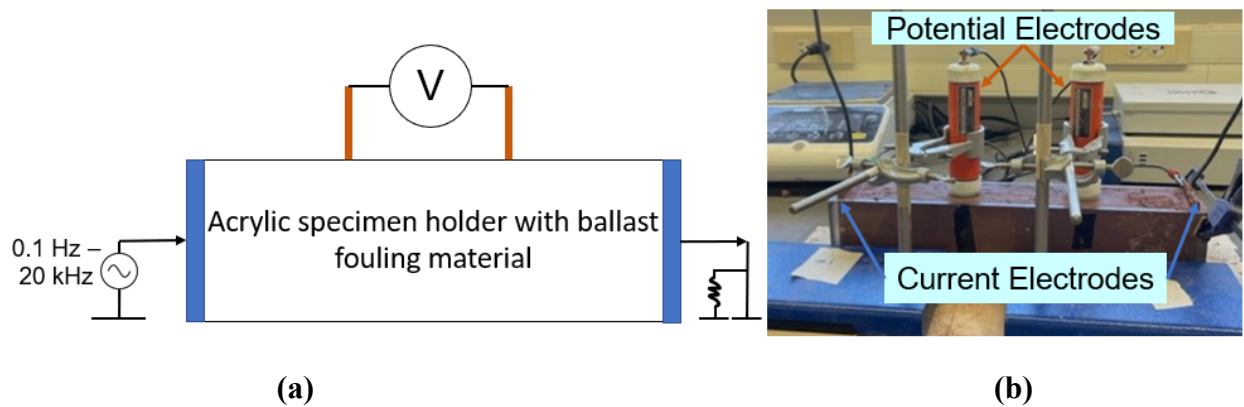
(a)   **(b)**

Figure 10: Complex impedance equipment for measuring ballast fouling materials: (a) schematic; (b) experimental set up

2.4.2 Testing Procedure

Researchers calibrated the current and potential electrodes using a standard calibration board provided with the equipment and then connected them to the Gamry Potentiostat 1010B. The team performed three tests on each specimen at sampling rates of 6, 8, and 10 samples per decade to assure ample data were measured. Team members conducted all experiments at 10 V peak-to-peak from 0.1 Hz to 20 kHz. All experimental design results are included in Appendix C. These include the effects of different current electrodes and potential electrodes as a function of saturation. Copper foam was ultimately used because it decreased the contact resistance between the fouling material and electrode. The results are repeatable until approximately 20 percent degree of saturation for sand, which had the poorest contact resistance. Researchers used RE-5 electrodes because the pellet electrodes were difficult to work with and several were damaged. The smaller RE-375 electrodes produced repeatable signals to the RE-5, however they were less stable in the potential electrode holders and this affected some results. The team validated the final experimental set up using a measured phase angle of tap water that was corrected for temperature and compared to a theoretical water test based on the conductivity of the water measured with a reference conductivity probe. The results of the water test as well as all experimental set up configurations are included in Appendix C. Final results for the sand fouling material as a function of saturation as well as the three fouling materials at two target degrees of saturation are presented herein.

3. Results and Analysis

3.1 LSDS Clean Ballast Results

To determine the experimental variability that is expected for clean ballast LSDS tests, the research team conducted two sets of replicate shear tests on a clean ballast specimen in a dry condition and a free drain (i.e., surface saturated or field capacity) condition, respectively. In both the dry and free drain conditions, researchers observed a high degree of similarity for the shear stress response curves in Figure 11(a) and (b). The overall response, as well as the peak shear stresses, were similar for the replicate tests either in dry or in free drained conditions. Additionally, the similarity can also be observed from Figure 11(c) and (d) where both the profile and the magnitude of the vertical displacement were consistent among the replicate tests under the same conditions. By conducting the replicate tests, the replicability of the measured results could be successfully evaluated and any measurements outside of this expected experimental variability could be said to be due to the presence of the fouling materials. Note that the shear stress increase in Figure 11(b) which occurred after approximately 100 mm of horizontal displacement for Replicate 1 was likely due to a larger particle located within the shear zone gap. This particle may have been jammed or positioned in such a way that it carried more stress until breaking and reducing the stress back to the expected value.
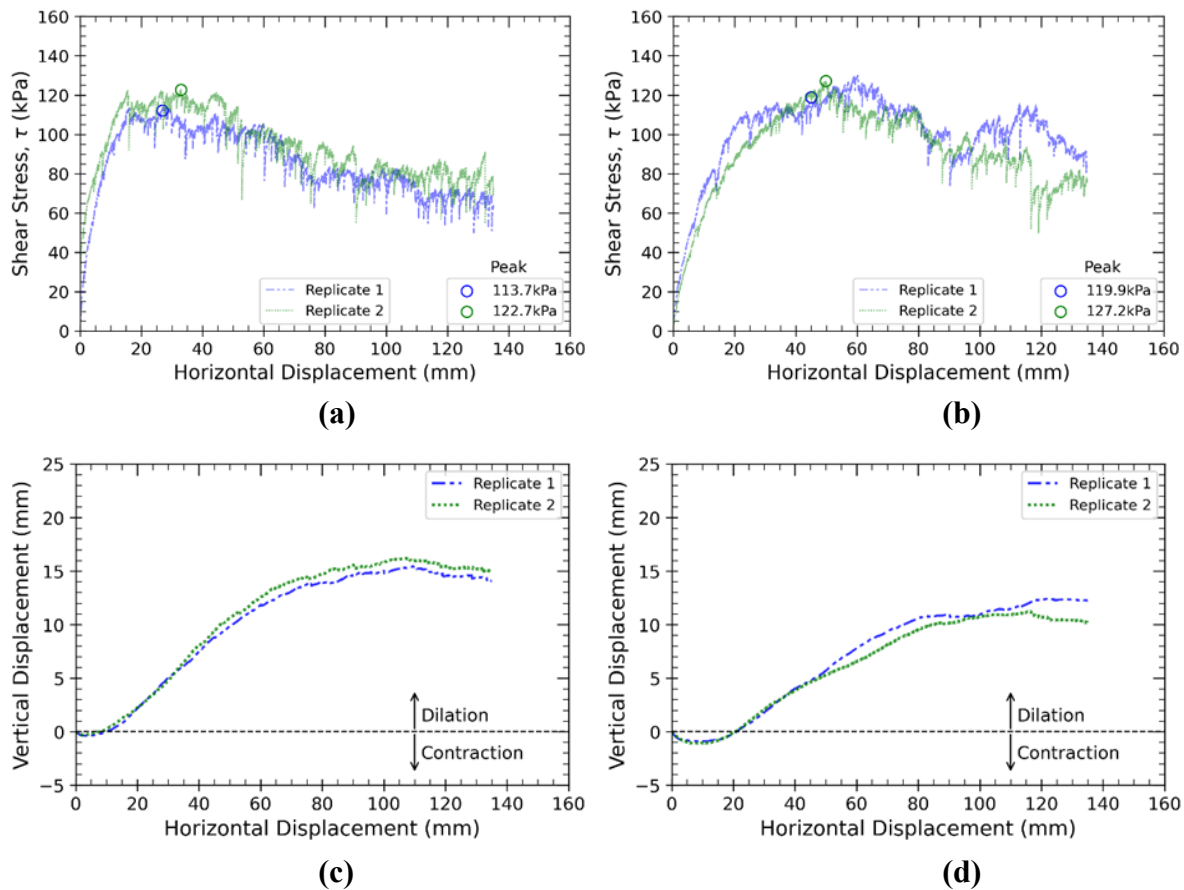

Figure 11: LSDS results for clean, granite ballast comparing dry and wet conditions: (a) dry shear stress response; (b) wet shear stress response; (c) dry vertical displacement; (d) wet vertical displacement

Team members performed additional tests to characterize the peak shear stress of clean basalt ballast as a function of water content. As shown in Figure 12, the clean basalt ballast behaved differently than the granite ballast. The peak shear stress of clean basalt ballast decreased as the water content increased. Compared to the very slight change in the peak shear stress of the granite ballast under dry and free-drained conditions, researchers observed a large change for the basalt, which indicated that the strength of the basalt ballast was more sensitive to the degree of water present. Note that only the dry and surface wet conditions were tested for the granite ballast as a part of the replicate tests and an intermediate point was not tested because the difference in peak shear stress was minimal.

Additionally, the plots of the shear stress and vertical displacement responses in Appendix B show that the magnitude of the shear stress varied significantly during the shear testing process. This "noise" suggests a higher brittleness of the basalt compared to the granite ballast at the same vertical stress. Considering the difference in results between the basalt and granite ballast, the findings obtained from the granite fouled ballast may not simply be applied to basalt ballast. Hence, more tests are needed to characterize the strength and volumetric response of basalt ballast under varying fouling and water content conditions.
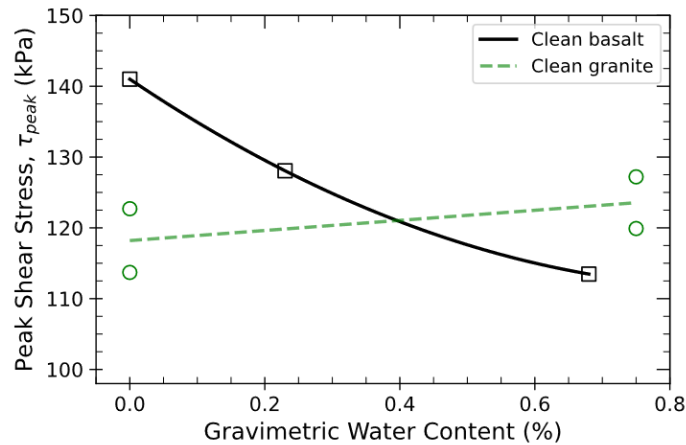

Figure 12: Comparison of the peak shear stress as a function of gravimetric water content between clean ballast and basalt

3.2 Fouled Ballast SWCC and LSDS Results

Researchers conducted laboratory experiments to investigate the evolution of the shear stress and volumetric deformation of fouled ballast as a function of the fouling material, fouling percent, and moisture content (as guided by SWCC results) to help improve the understanding of ballast degradation characteristics under varying conditions. At first, the residual suction of 3000 kPa was used as an approximation to fit all the datasets using Fredlund and Xing's three-parameter model. Such approximation eliminated the requirement for residual water content as a fitting parameter. This made it difficult to interpret hydraulic properties from the mathematical shape of the curve because the experiment showed that the residual suction of the fouled ballast was lower compared to other soil types. To avoid uncertainty in the predicted SWCC, the team used the four parameter Fredlund and Xing model to fit all SWCC datasets. The initial (i.e., fully saturated) volumetric water content was a function of the material type and the degree of fouling.

All fouled ballast SWCC results are presented in Appendix A. All LSDS testing results are presented in Appendix B. Major findings combing the two results are reported herein.

Figure 13 shows the results of the sand-fouled tests. The team allowed every SWCC test to free-drain and the reported "initial" volumetric water content was the first measured water content after ponded water was expelled from the stone. At the lowest end, Sand 1's 5 percent sand-fouled had an initial volumetric water content of 1 percent, with a residual 0.47 percent volumetric water content (Figure 13a). Sand 2's 15 percent sand-fouled had an initial volumetric water content of 4 percent, with a residual 0.52 percent volumetric water content. Despite the various degrees of fouling, Sand 1's 10 percent, Sand 2's 10 percent, and Sand 2's 15 percent plotted very close in terms of water retention, and the team observed very little difference between them. Figure 13b summarizes the relationship of the peak shear stress with the gravimetric water content, as guided by the SWCCs in Figure 13a under different sand fouling conditions. Note that volumetric water content could not be shown in this case because each specimen converted to a unique volumetric water content for the different fouling conditions. Overall, compared to the peak shear stress of the clean ballast as indicated by the green band range, the peak shear stress of the sand fouled ballast decreased with more sand fouling. However, it should be noted that the fouling material (differing by gradation in this case) affected peak stress differently. From the testing results, researchers inferred that the gradation of the fouling material was a key factor that should be taken into consideration when investigating the mechanical responses of the ballast. Therefore, simply using a geotechnical classification (e.g., SP for poorly graded sand) may not provide the full details needed to characterize or predict the behavior. Additionally, an increase in water content also resulted in a decrease in the peak shear stress for all fouling conditions. This decrease happened because increased water facilitated movement, rotation, and rearrangement of the ballast particles (i.e., lubricated the particles).
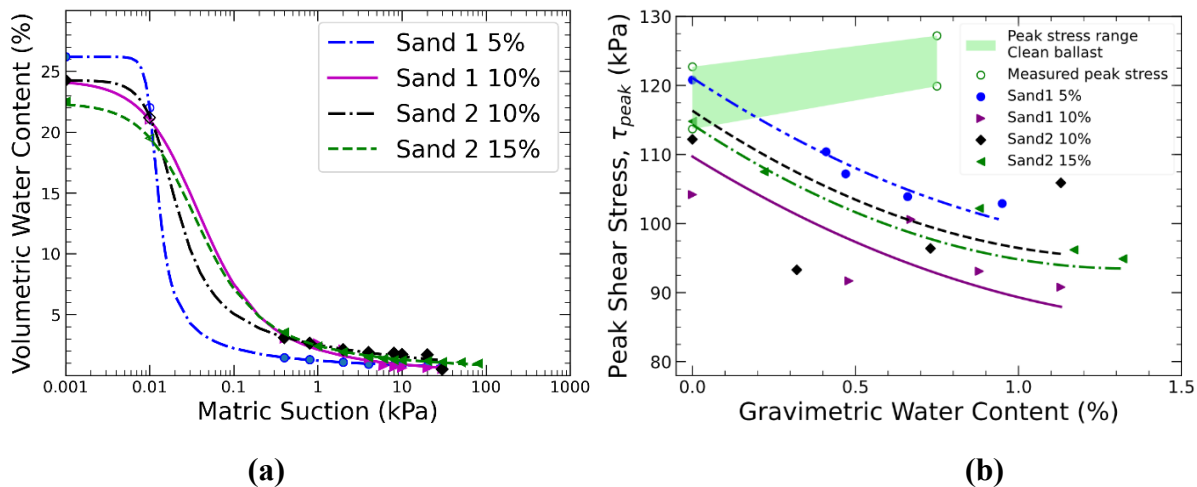

Figure 13: Sand fouling at 5%, 10%, and 15% degree of fouling: (a) SWCC results; (b) LSDS results

Figure 14a shows the results of the coal and clay-fouled SWCC tests. The 5 percent coal-fouled had an initial volumetric water content of 3 percent volumetric water content, with a residual 2.85 percent volumetric water content. The 10 percent coal-fouled had an initial volumetric water content of 8 percent, with a residual 7.33 percent volumetric water content. This was very similar to 10 percent clay (where the residual water content was 7.80 percent). The 15 percent

clay-fouled held an initial volumetric water content of 13.5 percent, with a residual 10.8 percent volumetric water content. Unfortunately, the team could not conduct a 15 percent coal test due to limited materials. Figure 14b shows the LSDS clay and coal-fouled ballast results. One notable feature that can be clearly observed is that as the fouling material percentage increased, the peak shear stress was reduced, and this reduction increased with increasing water content. Such reduction is likely because the fouling material coated the ballast particles and caused a decrease in the aggregate interlocking [34]. In comparing Figure 13b and Figure 14b, the team found that the coal fouling resulted in a larger decrease in peak shear stress compared to sand and clay fouling for each percentage of fouling. In fact, the specimen with 10 percent coal fouling which was considered moderately fouled showed a lower peak stress response overall than the specimen at 15 percent clay fouling which was considered fouled according to the FI and VCI. Note that both 10 percent coal and 15 percent clay were considered moderately fouled according to the RBF in Table 1.
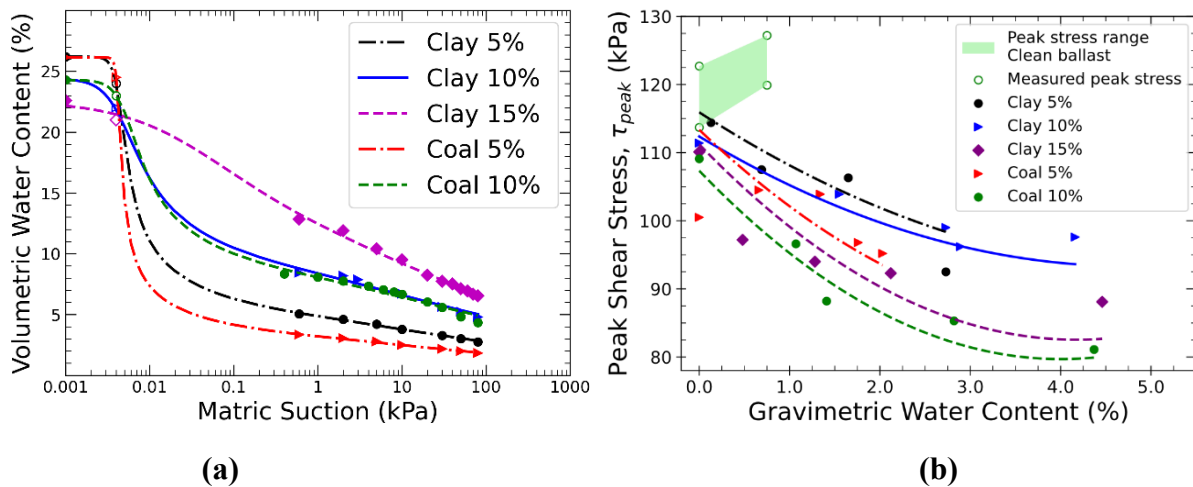
Figure 14: Coal and clay fouling at 5%, 10%, and 15% degree of fouling: (a) SWCC results; (b) LSDS results

For simplicity, Figure 15 compares the test results from the sand, clay, and coal-fouled ballast at 10 percent fouling condition. While there was an overall trend of decreasing peak shear stress with increasing water content, the team found that the greatest reduction in the peak shear stress was for the coal fouled specimens, even though at 10 percent fouling, the coal-fouled and clay-fouled specimens had very similar water retention capacities (Coal 10 percent residual water content 7.3 vs. 7.8 percent for Clay 10 percent). As shown in Figure 14a, the residual water content for coal at 5 percent is lower than clay at 5 percent (2.85 vs 4.35 percent). The team suspects that if it was possible to measure the SWCC for 15 percent coal, the residual water content would be higher than 15 percent clay. Based on these data, the residual water content was predicted as 11.8 percent for 15 percent coal fouling (by using the linear extrapolation method), and 15 percent clay fouling exhibited a residual water content of 10.8 percent. This phenomenon was likely due to the low specific gravity of pure coal (0.8-1.3) when compared to clay (2.3-2.7). Note that the specific gravity of the coal tested was not this low because it was mostly sand (approximately 52 percent sand sized particles as shown in Figure 2); however, the relatively lower specific gravity meant there was an increased volume of coal fouling materials as the degree of fouling increased [35].

The loss of peak shear stress at 10 percent suggests that coal fouling caused the shear strength of the ballast to deteriorate much more than clay and that there may be a higher volume of coal than clay at this target degree of fouling. Furthermore, Huang et al. [36] pointed out that coal dust was the worst fouling agent for its impact on track substructure and roadbed, and it caused the most drastic decreases in shear strength, especially at high fouling levels. Their findings are consistent with those from this research. It is also interesting to note the low peak stress values for the 10 percent sand fouled specimens in Figure 15. Although the water content range was small for these specimens and the coal fouling eventually reduced the peak stress further at higher water contents, the sand fouled specimens had a drastic effect on peak stress response in the drier conditions. While the coal fouling may have provided a type of lubricating effect, the sand fouling perhaps reduced interlocking as sand particles provided a rolling mechanism at ballast contacts. This is also further complicated by the fact that most in service coal fouling, like the material examined in this study, also contains sand particles. More research is needed to further understand the mechanisms driving this reduction in interlocking and peak shear stress.
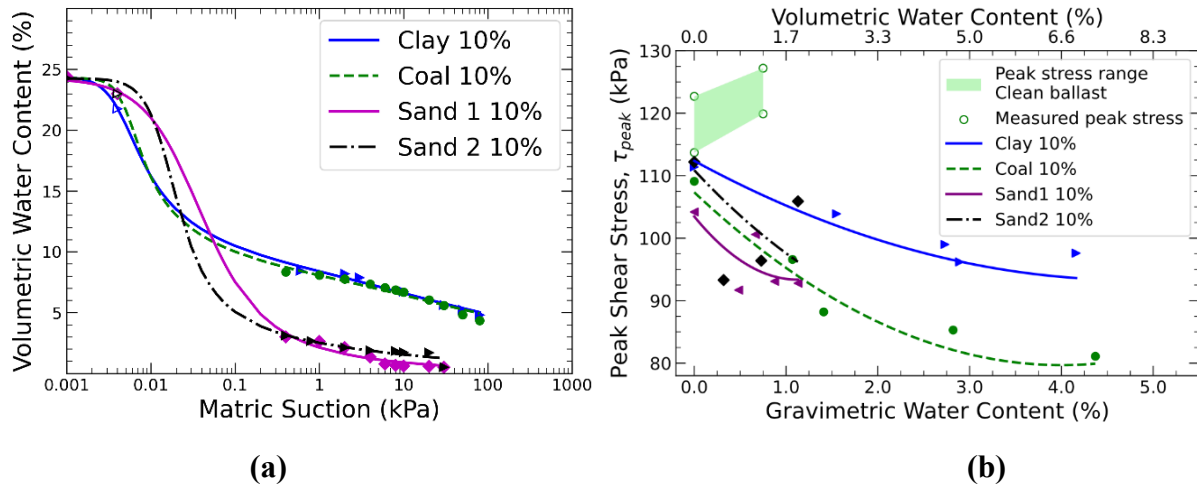
Figure 15: Comparison of the 10% fouled ballast: (a) SWCC results; (b) LSDS results

3.3 Complex Impedance Results

Upon finalizing the experimental set up and testing protocol, the team tested the complex impedance of three ballast fouling materials at fully saturated and various degrees of saturation. The three materials were the coal, clay, and Sand 2 specimens used for the LSDS and SWCC experiments. Sand 1 was not tested because the material was not available after creating the Sand 2 mixture by combining two breakdown ballast samples. The variables in Figure 16 that define the sample preparation characteristics include the degree of saturation, S, the volumetric water content, θ, and the specimen dry density, ρ_d. Both the degree of saturation, S, and volumetric water content, θ, are reported to link the complex impedance results where the team controlled saturation to the SWCC and LSDS results. Figure 16 shows the results of Sand 2 from 99 percent saturated (noted as $\theta = 28$ percent) to 23 percent saturated (noted as $\theta = 6$ percent), including replicates near saturation (noted as $\theta = 21$ - 28 percent). The saturated specimens showed a near constant phase angle response from 0.1 Hz to 20 kHz. In other words, when compared to the water test in Appendix C, the phase angles versus frequency were similarly relatively low because dipolar polarization of water molecules occurs at higher frequencies (i.e., $f > 10^8$ Hz).

Furthermore, sands are relatively non-polarizable and thus the water largely controlled the near constant response. The unsaturated results at θ = 8 percent and θ = 6 percent may have exhibited a peak frequency response as expected in the absence of electron conducting minerals. However, the anticipated peak was not captured in this frequency range. Researchers are currently exploring frequency-dependent mechanistic models to describe this response. The unsaturated results became very erratic below 20 percent saturation, as shown in Appendix C. The team also observed this erratic response in the coal specimens below 20 percent. Therefore, researchers tested all specimens at full saturation and approximately 40 percent saturation so that the results could be compared to the phase angle response of the sand in Figure 16.
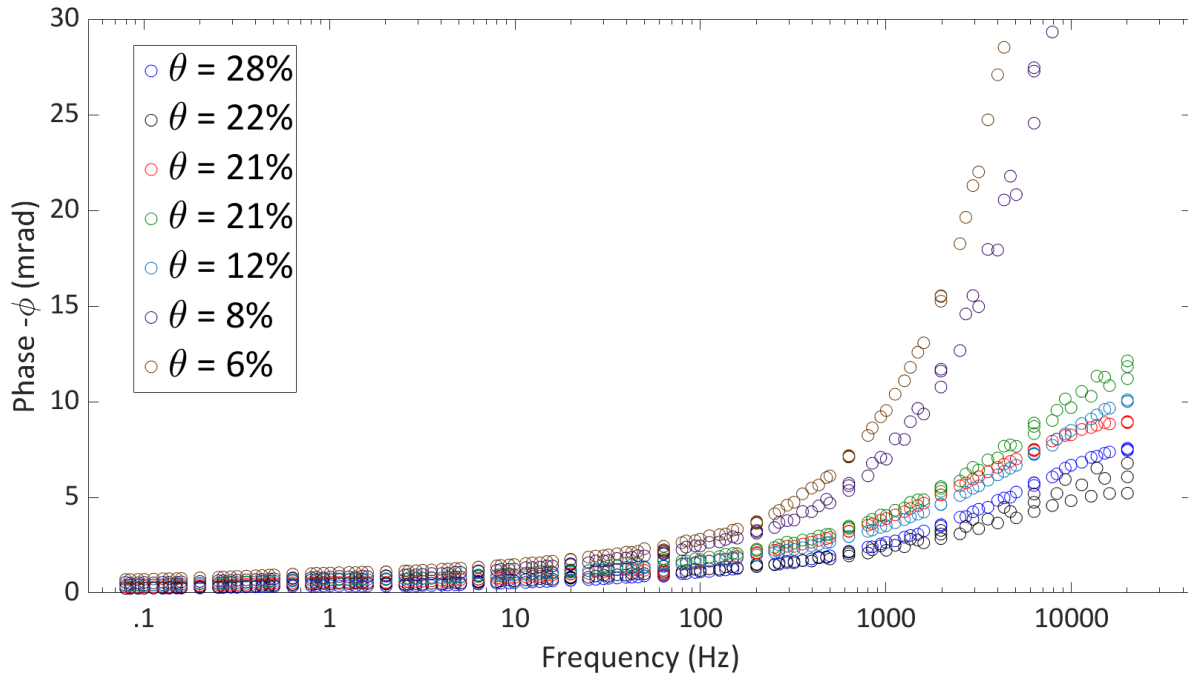
Figure 16: Sand 2 at six volumetric water contents using copper foam electrodes to show the effect of degree of saturation: θ=28% (99% saturated, $\rho_d = 1.89$ g/cc; θ=12% (43% saturated, $\rho_d = 1.89$ g/cc); θ=6% (23% saturated, $\rho_d = 1.88$ g/cc)

Figure 17 shows the measured phase angle for the three fouling materials at 100 percent saturation and 40 percent saturation. In both cases, clay had the highest response, fully saturated and at 40 percent due to the high concentration of bound negative charges in clay. Although not a natural clay, the manufactured clay still had an overall bound negative charge that enhanced cation transport relative to anion transport. Note that a natural clay would have a greater phase angle response at higher frequencies, and this varies based on the clay mineralogy. The clay particles result in membrane-type polarization that is associated with cation transport in the electrical double layer surrounding the clay particles. In the case of the clay, the fully saturated specimen had the highest phase response. This is likely because when fully saturated the clay had a more uniform and larger adsorbed layer which contributed to the ease of cation transport in the electrical double layer within the clay fabric.

The fully saturated sand and coal (i.e., coal θ = 46 percent, sand θ = 28 percent) had relatively low phase responses and were very similar with a near constant phase angle. In these cases, the

effects of the water (which was low polarizable at these frequencies) was controlling the response as opposed to electrical double layer mechanisms. The unsaturated results of the coal and sand show divergence around 200 Hz, where the phase angle response of the coal was greater than the sand. This is likely due to the electron conducting particles in the coal specimens. Recall that the coal specimens were mostly sand (see Figure 2), thus even a small amount of coal dust was detectable with this measurement in the unsaturated condition. The next step of this research will be to evaluate frequency-dependent mechanistic models to describe the polarization mechanisms more fully in the specimens and to determine the interparticle characteristics that lead to a different response. At this time, a preliminary Cole-Cole model [37] appears to fit the saturated data well.
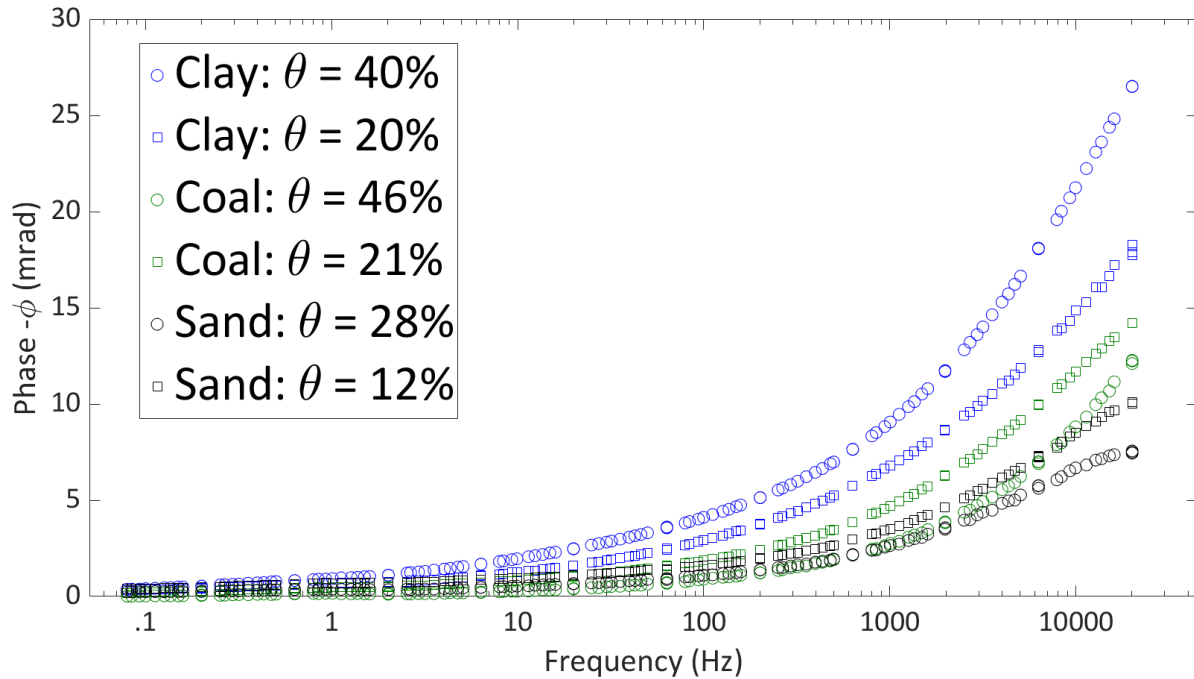
Figure 17: Complex impedance of three fouling materials near fully saturated and 43±2%: Clay $\theta = 40\%$ (96% saturation, $\rho_d = 1.59$ g/cc); Clay $\theta = 20\%$ (45% saturated, $\rho_d = 1.58$ g/cc); Coal $\theta = 46\%$ (96% saturated, $\rho_d = 1.37$ g/cc); Coal $\theta = 21\%$ (42% saturated, $\rho_d = 1.37$ g/cc); Sand $\theta = 28\%$ (99% saturated, $\rho_d = 1.89$ g/cc); Sand $\theta = 12\%$ (43% saturated, $\rho_d = 1.89$ g/cc)

3.4 Discussion

The SWCC and LSDS results individually showed trends that were expected and followed previous researchers' findings; however, when combined and analyzed with the complex impedance results, several interesting features were discovered. As discussed, the residual water contents for clay and coal fouling at 10 percent were nearly identical. Yet the peak stress response in the unsaturated range was drastically different, with coal showing the greatest peak stress loss with increasing moisture content. Another interesting finding was the large reduction in peak stress for the sand fouling at 10 percent, although it exhibited very low residual water content and was tested at a very low water content range. Therefore, the air entry and residual

26

water contents from the SWCCs did not uniquely and fully describe the measured strength loss. The fact that sand fouling caused such a reduction in peak stress means that there was likely a rolling or similar type of mechanism enacted by the small particles at the microscale level that reduced the ballast-to-ballast interlocking, as inadequate interlocking allows aggregates to easily move and slide over one another. The coal fouling being comprised of over 52 percent sand sized particles (from in service ballast breakdown) likely also produced this rolling mechanism, along with an additional lubrication feature that contributed to peak stress loss at higher moisture contents. There was also a higher volume of coal fouling present because of the specific gravity differences, but more work will be needed to determine the actual volumetric quantity of coal present. The clay specimens also likely had the lubricating feature from the clay particles as moisture contents increased, but there was not enough clay present to greatly reduce the interlocking from ballast-to-ballast contacts. The clay fouling may have also resulted in a higher unsaturated strength compared to other fouling types due to interparticle forces and apparent cohesion caused by suction, but it is difficult to make a definitive conclusion given these data.

This study is unique because of the added information provided by the complex impedance results. At this stage, the measured phase angles of the three ballast materials in the unsaturated condition showed promise as an indicator of material type. The measured volumetric moisture contents for clay and coal at fully saturated and 40 percent degree of saturation were quite similar, yet the phase responses were notably different. Thus, the effects of the amount of water in these two specimens can be removed from consideration. As shown in Figure 14b, there was a significant loss of peak shear stress in the coal relative to the clay at similar water contents. Based on these data, note that the complex impedance measurements were capable of differentiating different fouling materials. It is interesting that both the peak shear stress and complex impedance measurements of coal were relatively lower than clay. This is likely due to the different interfaces between the particles, both within the fouling materials themselves and fouling material-ballast particle interfaces. Whether these interfaces also yield different interparticle forces cannot be differentiated yet being able to identify different unsaturated materials with complex impedance shows promise in this direction. Additional research should consider different clay mineralogies, such as Montmorillonite and Illite, to determine whether there is a relationship with the high electromagnetic response based on the electrical double layer and the peak stress. The complex impedance results also show that adsorbed water in the electrical double layer was likely another contributing factor. Clay contains greater amounts of bound water and the material itself exhibits a relatively higher phase angle response. Because sand is a very low polarizable material, there is not much insight gained through electromagnetics at these frequencies and the results are similar to what is measured with pure water. This feature helps qualitatively distinguish sand from clay fouling in both saturated and unsaturated conditions, which is difficult with single frequency measurements. This is further strengthened by the low residual water content measured in the SWCC for sand which indicates that there was not an increase in strength from negative pore water pressure and that the mechanical response was simply a function of particle interactions.

The team found the complex impedance response for the coal fouling material very interesting. The coal sample was 52 percent sand sized particles, and X-ray diffraction (XRD) results of coal passing the No. 200 sieve showed that the fine particles were comprised of 52 percent carbon. Fully saturated, the coal phase angles were similar to sand; however, when tested under unsaturated conditions, the coal exhibited a different response compared to sand and clay. These differences may have been due to different electron conducting particles in the coal specimens.

Thus, even small amounts of coal dust can be identified using unsaturated complex impedance measurements. This indicates that complex impedance may provide a unique identifier with which the resulting material mechanical performance can be related. These results highlight the potential for using complex impedance to identify different interparticle forces, which likely control the peak shear stress response. A summary of findings outlined in this discussion is shown in Table 2. More research is needed, however, to further understand the response from additional fouling "mixtures" (e.g., a sandy clay fouling material) to determine whether there is a relationship that can be distinguished in terms of electromagnetics and strength. In other words, it is not clear whether a sandy clay-fouled specimen, for example, will exhibit a similar response to a coal fouled specimen in terms of 1) peak stress reduction due to the combined rolling and lubricating mechanisms at the ballast contacts, and 2) complex impedance where a portion of the sample is highly conductive with a strong phase lag response (i.e., clay) while the other is not (i.e., sand).

Table 2: Summary of findings relevant to the measurement methods and materials in this two-phase study

Measurement Type	Summary of Findings				
	Advantages	Disadvantages	Clay	Coal	Sand
SWCC	Relates fouled ballast matric suction and moisture content, measures hydraulic properties of fouled ballast	Water storage potential alone did not uniquely identify a corresponding stress reduction and could not distinguish between all fouling types	Highest residual moisture content and range of suction	Highest increase in residual moisture content with fouling	Lowest residual moisture content
LSDS	Provides a quantitative assessment of strength under varying moisture and fouling conditions and can indicate conditions which may be more problematic	Shearing conditions are not identical to the expected field conditions and strength cannot be used as a rapid detection method in the field	Highest peak shear stress across a wide range of moisture contents	Greatest peak shear stress loss likely due to a combination of rolling and lubrication at the ballast particle contacts	Lowest unsaturated peak shear stress over a small range of lower moisture contents; however, the coal had lower peak shear stress values at higher water contents
Complex Impedance	Provides a measure of the electrical response of a material at different frequencies and shows promise as a unique indicator and detection technique	The current setup is limited to ballast fouling materials; ballast must be included to translate to in situ measurements	Highest phase angle	Greatest discernable difference in saturated and unsaturated conditions, discernable from sand with this measurement	Lowest phase angle, similar response to water thus can be distinguished from clay and coal

4. Conclusion

Researchers from Kansas State University and the University of Arkansas worked to identify the factors that contribute to ballast strength loss due to fouling. In Phase I, the team established the SWCCs of fouling materials as well as the experimental design for measuring fouled ballast SWCCs and shear stress and volumetric response. In this Phase II study, the team used the validated large-scale devices to measure the SWCCs and peak shear stress of ten fouled ballast specimens. Researchers used the SWCC results to guide specimen preparation at target volumetric water contents for LSDS experiments and the results were presented together to describe relationships between the low residual water contents in fouled ballast and the measured peak shear stress. A unique finding is that a fourth correction parameter in SWCC modeling cannot be neglected in these specimens, as is common practice in soils. The LSDS results highlight that increasing water content decreases the measured peak shear stress for all specimens. Of the four fouling materials, the two sand fouled specimens highlight the influence of gradation on peak shear stress. The team observed low peak shear stress in sand even though these specimens were tested at very low water contents. Researchers concluded the loss of peak shear stress in sand is due to particle interactions rather than an increase in strength from negative porewater pressure. The clay fouled specimens had the highest residual water content of all specimens as well as the highest unsaturated strength, possibly due to interparticle forces and apparent cohesion caused by suction in this material. The team observed the greatest loss in peak shear stress in the unsaturated coal fouled specimens, which was similarly observed by previous researchers. Additionally, clean basalt ballast exhibited a decrease in peak stress with increasing moisture content while granite ballast did not show a reduction from the presence of water. More work is needed to understand the different particle interaction mechanisms for the basalt and the added effects from fouling.

The research team conducted complex impedance measurements to describe the electromagnetic response of ballast fouling materials. Most of the complex impedance results were system to measure unsaturated specimens, while most complex impedance testing is on saturated rock core specimens. The team established how to reliably measure the complex impedance of ballast fouling materials from fully saturated to approximately 20 percent saturation. One component of complex impedance, the real component, is a material property measured by GPR. Researchers collected broad-spectrum complex impedance measurements to decouple difficulties in GPR signals that often arise when specimens are fully saturated. The results show that fully saturated clay fouling materials have the highest measured phase angle response, as expected due to the electrical double layer in clays. There was a negligible difference between the fully saturated sand and coal specimens, which shows the difficulty of discerning these two saturated materials. The unsaturated measurements provided unique signals for all materials. At this point, the team offers a qualitative interpretation based on the measured phase angles and notes that this measurement has the potential to discern different fouling materials. The differences in the complex impedance responses were likely due to differences at particle-to-particle interfaces. These results highlight the potential for using complex impedance to identify different interparticle forces, which likely control the variable peak shear stress response as a function of moisture and the degree of fouling. More work is needed to develop a phenomenological model to describe the polarization mechanisms of the unsaturated materials. This study shows the potential for broad spectrum complex impedance measurements to support ground penetrating

radar in the field with a full wave form inversion to rapidly identify the type of fouling, degree of fouling, and loss of strength due to fouling.

5. References

[1] Hyslip, J. P., Olhoeft, G. R., Selig, E. T., & Smith, S. S. (2005). *Ground Penetrating Radar for Railroad Track Substructure Evaluation* (DOT/FRA/ORD-05/04). Federal Railroad Administration.

[2] Conti, M., de Castro, D., Bezerra, F., & Cazarin, C. (2019). Porosity estimation and geometric characterization of fractured and karstified carbonate rocks using GPR data in the Salitre Formation, Brazil. *Pure and Applied Geophysics, 176*(4), 1673-1689.

[3] Clark, M., Gillespie, R., Kemp, T., McCann, D., & Forde, M. (2001). Electromagnetic properties of railway ballast," *NDT & E International, 34*(5), 305-311.

[4] Alsabhan, A., Fratta, D., Warren, B. J., Tinjum, J. M., & Edil, T. B. (2019). Using time domain reflectometry to determine depth of fouling and fouling type in railway track substructure. *Geotechnical Testing Journal, 42*(1), 156–179.

[5] Sussmann, T. R., O'Hara, K. R., & Selig, E. T. (2002). Development of material properties for railway application of ground-penetrating radar. *Ninth International Conference on Ground Penetrating Radar*, Santa Barbara, California.

[6] Klotzsche, A., Vereecken, H., & van der Kruk, J. (2019). Review of crosshole ground-penetrating radar full-waveform inversion of experimental data: Recent developments, challenges, and pitfalls. *Geophysics, 84*(6), H13-H28.

[7] Lavoue, F. (2014). Two-dimensional permitivity and conductivity imaging by full waveform inversion of multioffset GPR data: A frequency-domain quasi-Newton approach. *Geophysics Journal International, 197*(1), 248-268.

[8] Kulesza, S., Barry, M., Sherwood, R., & Santos, A. (2022). Unsaturated Characteristics of Fouled Ballast to Support In Situ Identification of Fouling using Ground Penetrating Radar – Phase I. (DOT/FRA/ORD-22/09). Federal Railroad Administration.

[9] Sherwood, R., Kulesza, S., & Bernhardt-Barry, M. (2020). Unsaturated characteristics of fouled ballast to support in situ identification of fouling. *Geo-Congress 2020*, Minneapolis.

[10] Fredlund, D. G., & Rahardjo, H. (1993). Soil mechanics for unsaturated soils. John Wiley & Sons.

[11] ASTM (2020). ASTM C136 Standard Test Method for Sieve Analysis of Fine and Coarse Aggregates. *ASTM International, 04*(02).

[12] AREMA (2019). Chapter 1 Railway and Ballast. *AREMA Manual for Railway Engineering*. American Railway Engineering and Maintenance-of-Way Association (AREMA).

[13] ASTM (2016). D4254 Standard Test Methods for Minimum Index Density and Unit Weight of Soils and Calculation of Relative Density. ASTM International.

[14] ASTM (2019). D4253 Standard Test Methods for Maximum Index Density and Unit Weight of Soils Using a Vibratory Table. ASTM International.

[15] Selig, E. T., & Waters, J. M. (1994). Track geotechnology and substructure management. Default Book Series.

[16] Indraratna, B., Nimbalkar, S., & Tennakoon, N. (2010). The behavior of ballasted track foundations: Track drainage and geosynthetic reinforcement. *ASCE GeoFlorida*, Orlando.

[17] Indraratna, B., Su, L.-j., & Rujikiatkamjorn, C. (2011). A new parameter for classification and evaluation of railway ballast fouling. *Canadian Geotechnical Journal, 48*, 322–326.

[18] Wayllace, A., & Lu, N. (2012). A transient water release and imbibitions method for rapidly measuring wetting and drying soil water retention and hydraulic conductivity functions. *Geotechnical Testing Journal, 35*(1), 103–117.

[19] Hilf, J. (1956). An investigation of pore-water pressure in compacted cohesive soils (Ph.D. Thesis). University of Colorado.

[20] Van Genuchten, M. T. (1980). A closed-form equation for predicting the hydraulic conductivity of unsaturated soils. *Soil science society of America journal, 44*(5), 892-898.

[21] Leong, E. C., & Rahardjo, H. (1997). Review of soil-water characteristic curve equations. *Journal of geotechnical and geoenvironmental engineering, 123*(12), 1106-1117.

[22] Fredlund, D. G., & Xing, A. (1994). Equations for the soil-water characteristic curve. *Canadian geotechnical journal, 31*(4), 521-532.

[23] Li, X., Li, J. H., & Zhang, L. M. (2014). Predicting bimodal soil–water characteristic curves and permeability functions using physically based parameters. *Computers and geotechnics, 57*, 85-96.

[24] Sarker, D., & Wang, J. X. (2022). Experimental Study on Soil–Water Retention Properties of Compacted Expansive Clay. *Advances in Transportation Geotechnics IV*, Springer, 433-445.

[25] Stark, T. D. (2014). Ballast direct shear testing. *2014 Joint Rail Conference*, Colorado Springs, CO.

[26] Estaire, J., & Santana, M. (2018). Large direct shear tests performed with fresh ballast. *Railroad Ballast Testing and Properties, ASTM STP1605,* 144-161.

[27] Indraratna, B., Ngo, N., & Vinod, R. C. & J. S. (2014). Behavior of fresh and fouled railway ballast subjected to direct shear testing: discrete element simulation. *International Journal of Geomechanics, 14*(1), 34-44.

[28] Sevi, A., Ge, L., & Take, W. (2009). A large-scale triaxial apparatus for prototype railroad ballast testing. *Geotechnical Testing Journal, 32*(4), 297-304.

[29] ASTM (2014). Standard Test Method for Direct Shear Test of Soils Under Consolidated Drained Conditions. ASTM International.

[30] Ghazavi, M. (2004). Shear strength characteristics of sand mixed with granular rubber. *Geotechnical & Geological Engineering, 22*, 401-416.

[31] Knight, R. J., & Endres, A. L. (2005). An introduction to rock physics principles for near-surface geophysics. *Near-surface geophysics*, Society of Exploration Geophysicists.

[32] Zimmermann, E., Kemna, A., Berwix, J., Glaas, W., Münch, H., & Huisman, J. A high-accuracy impedance spectrometer for measuring sediments with low polarizability. *Measurement Science and Technology, 19*(10), 105-603.

[33] Vanhala H., & Soininen, H. (1995). Laboratory techniques for measurement of spectral inducted polarization (SIP) response of soil samples. *Geophysical Prospecting, 43*, 655-676.

[34] Danesh, A., Palassi, M., & Mirghasemi, A. A. (2018). Effect of sand and clay fouling on the shear strength of railway ballast for different ballast gradations. *Granular Matter, 20*, 1-14.

[35] Sussmann, T. R., Ruel, M., & Chrismer, S. M. (2012). Source of ballast fouling and influence considerations for condition assessment criteria. *Transportation Research Record, 2289*, 87-94.

[36] Huang, H., Tutumluer, E., & Dombrow, W. (2009). Laboratory characterization of fouled railroad ballast behavior. *Transportation research record, 2117*(1), 93-101.

[37] Dias, C. (2000). Developments in a model to describe low-frequency electrical polarization of rocks. *Geophysics, 65*(2), 437-451.

Appendix A.
SWCC Results

Table A.1: Fouled ballast specimen hydraulic parameters

Sample type	θ_r	θ_s	a	n	m	SSE
Sand 1 5%	0.47	26.18	0.011	7.659	0.867	0.005
Sand 1 10%	2.26	24.25	0.026	1.328	1.502	0.917
Sand 2 10%	1.99	24.25	0.013	2.815	0.899	0.720
Sand 2 15%	0.52	22.38	0.023	1.409	1.326	0.091
Coal 5%	2.85	26.14	0.004	19.960	0.443	0.012
Coal 10%	7.33	24.28	0.005	4.163	0.348	0.989
Clay 5%	4.35	26.19	0.004	8.266	0.435	0.028
Clay 10%	7.80	24.38	0.004	2.989	0.369	0.451
Clay 15%	10.79	22.58	0.017	0.772	0.488	0.861

θ_s – Saturated volumetric water content
θ_r – Residual volumetric water content
a, n, m – Fredlund and Xing fitting parameters
SSE – Sum of squared errors
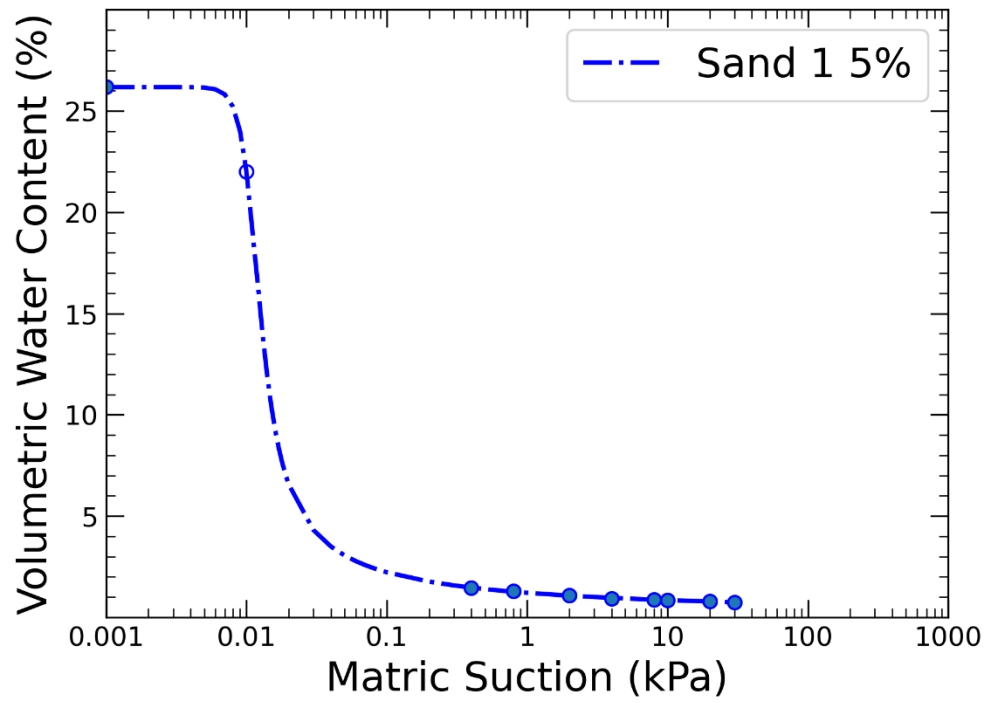
Figure A.1: Sand 1 5% SWCC
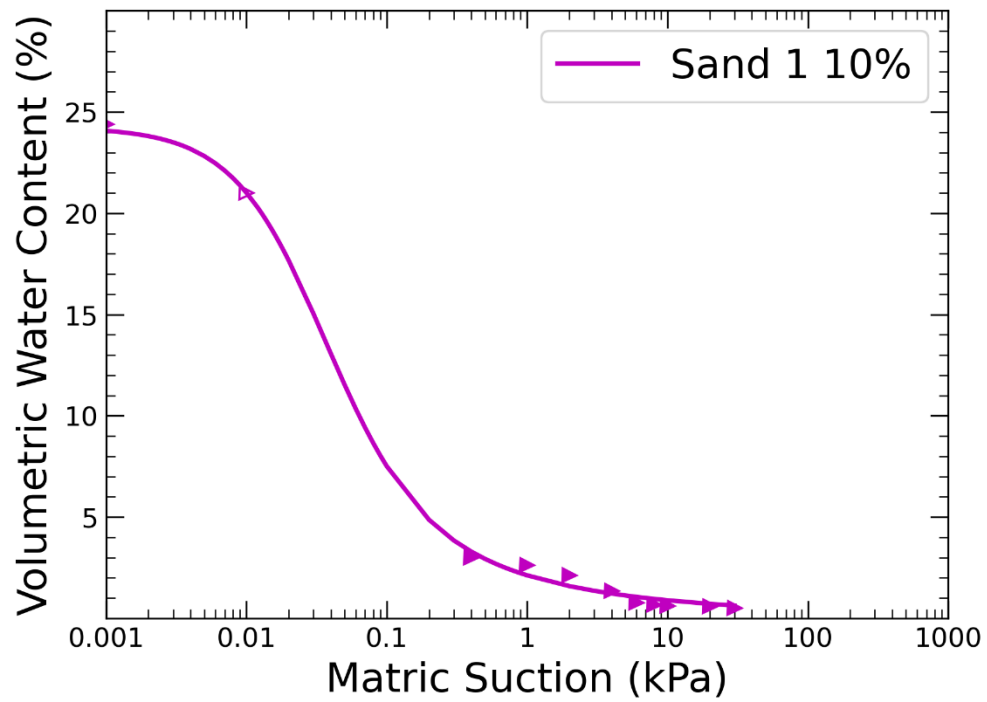
Figure A.2: Sand 1 10% SWCC
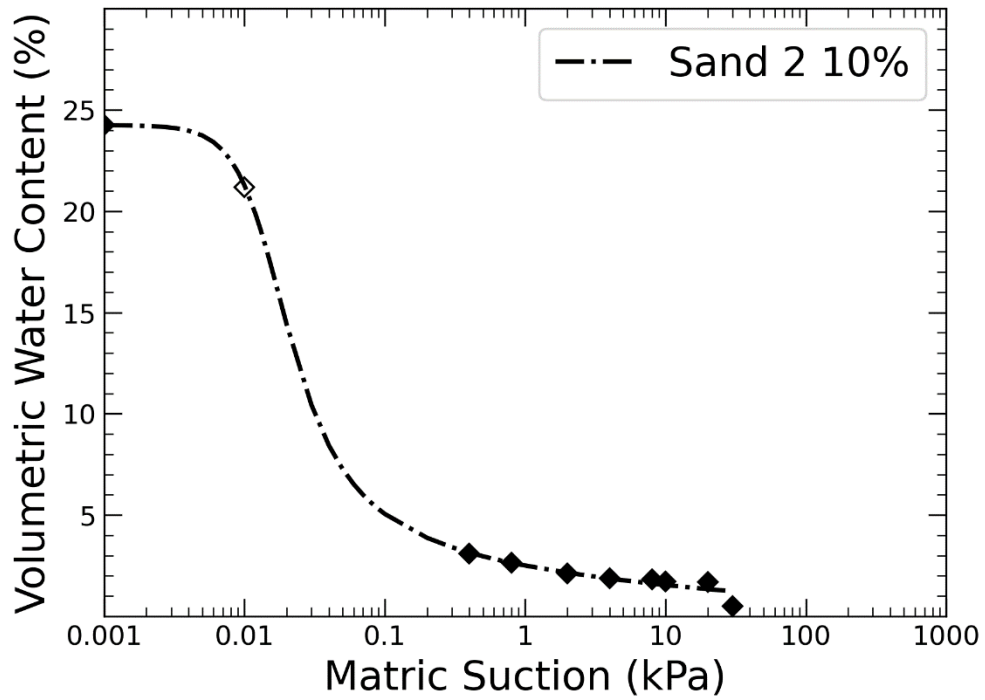
Figure A.3: Sand 2 10% SWCC
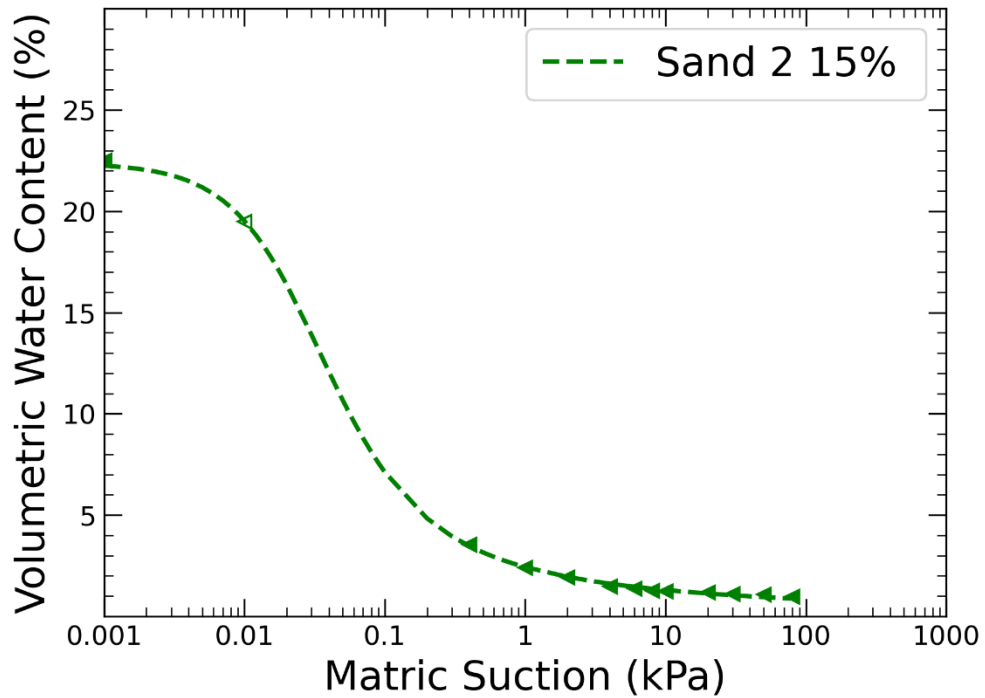
Figure A.4: Sand 2 15% SWCC
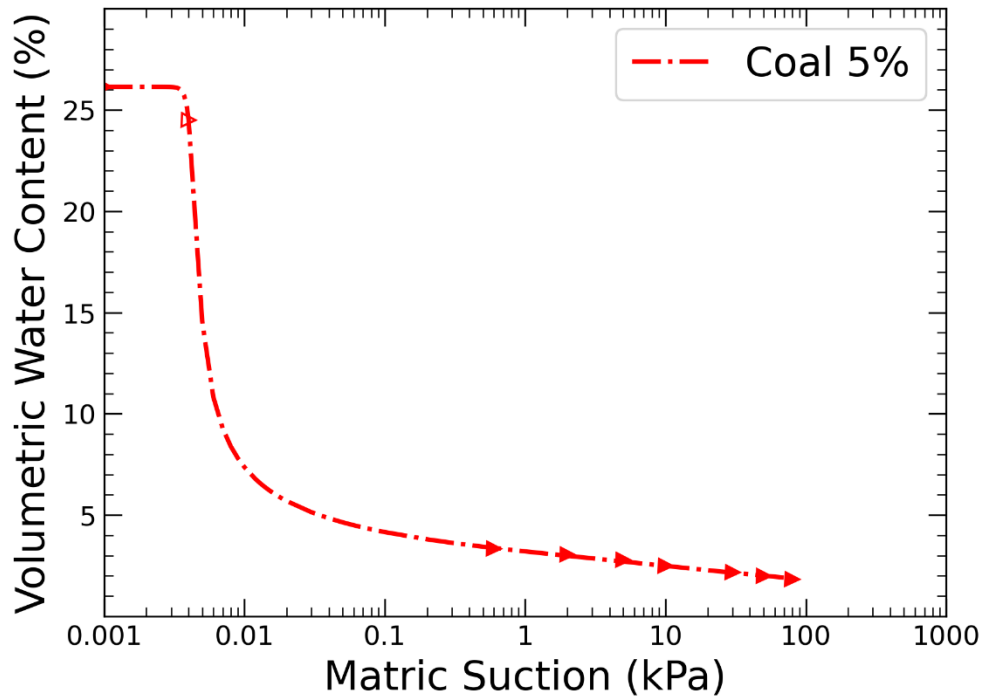
Figure A.5: Coal 5% SWCC
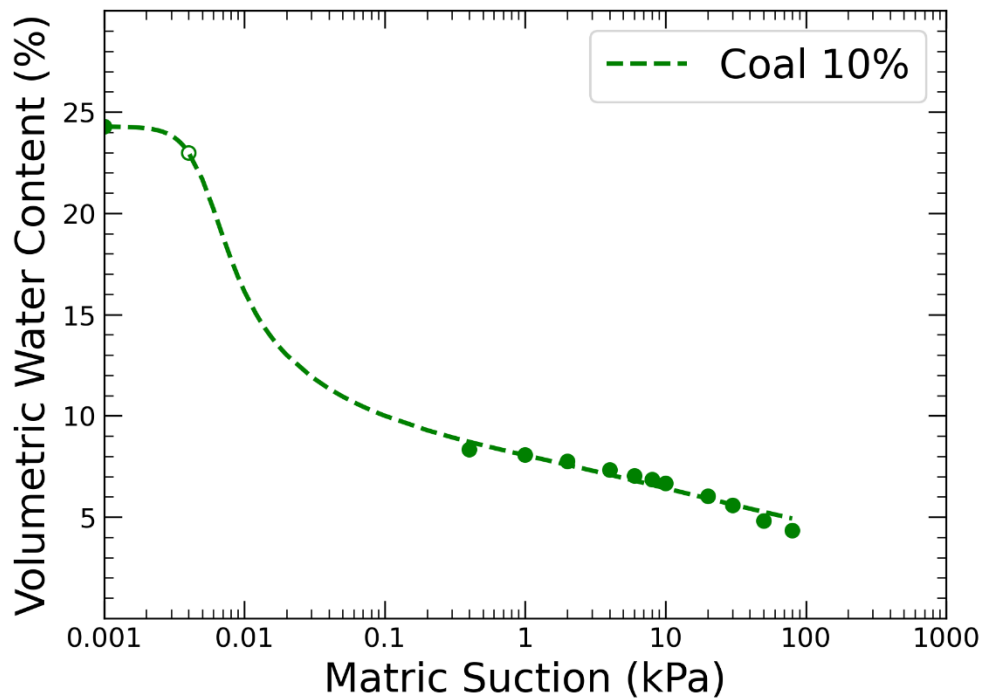
Figure A.6: Coal 10% SWCC
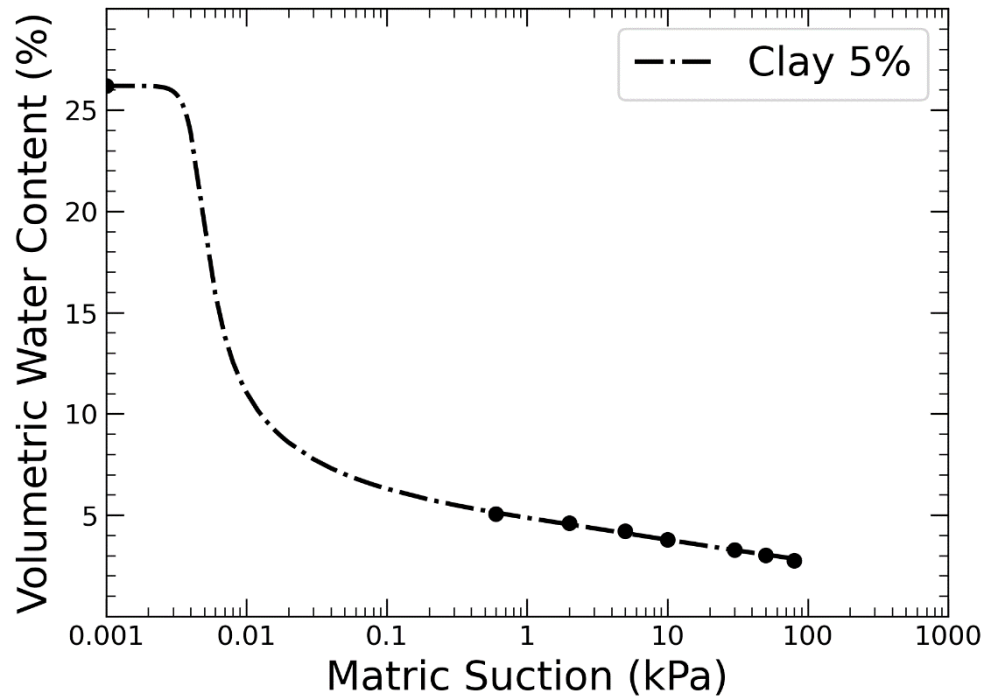
Figure A.7: Clay 5% SWCC
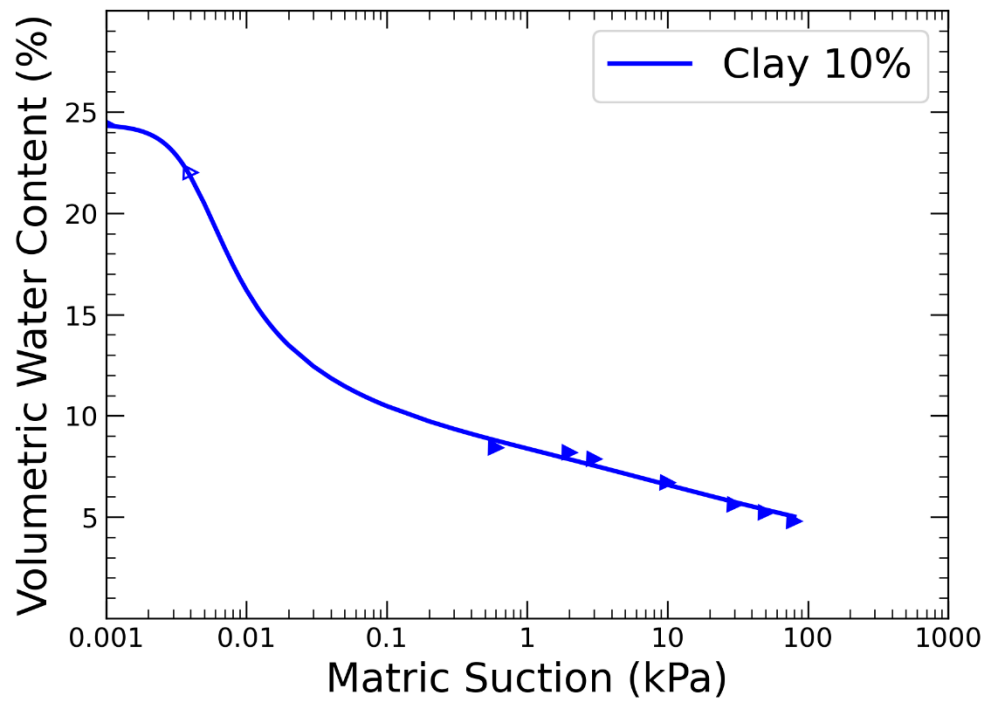
Figure A.8: Clay 10% SWCC
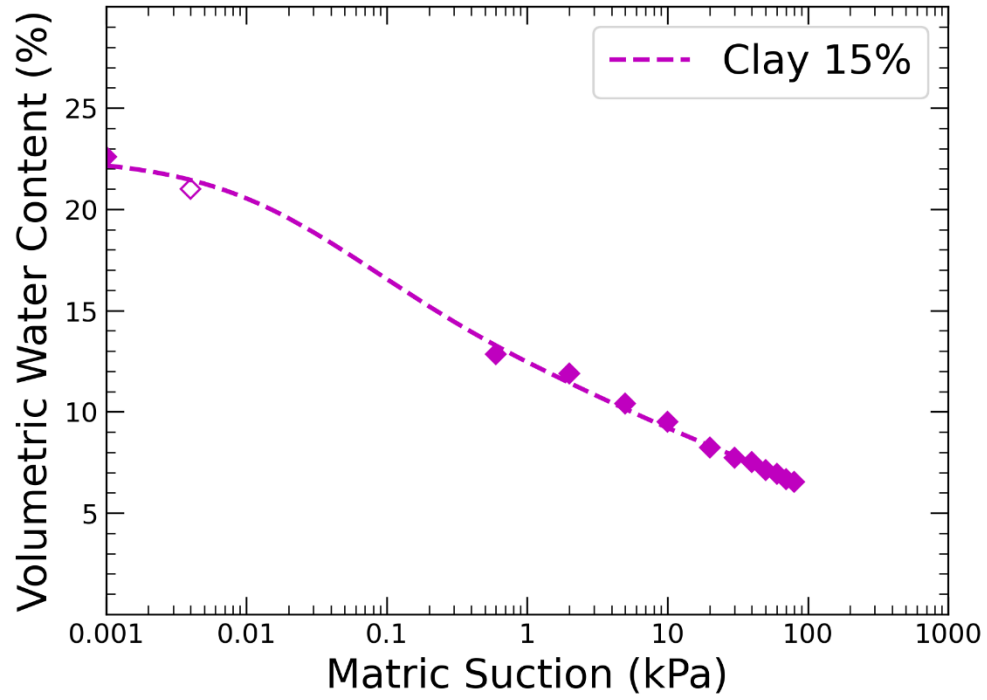
Figure A.9: Clay 15% SWCC
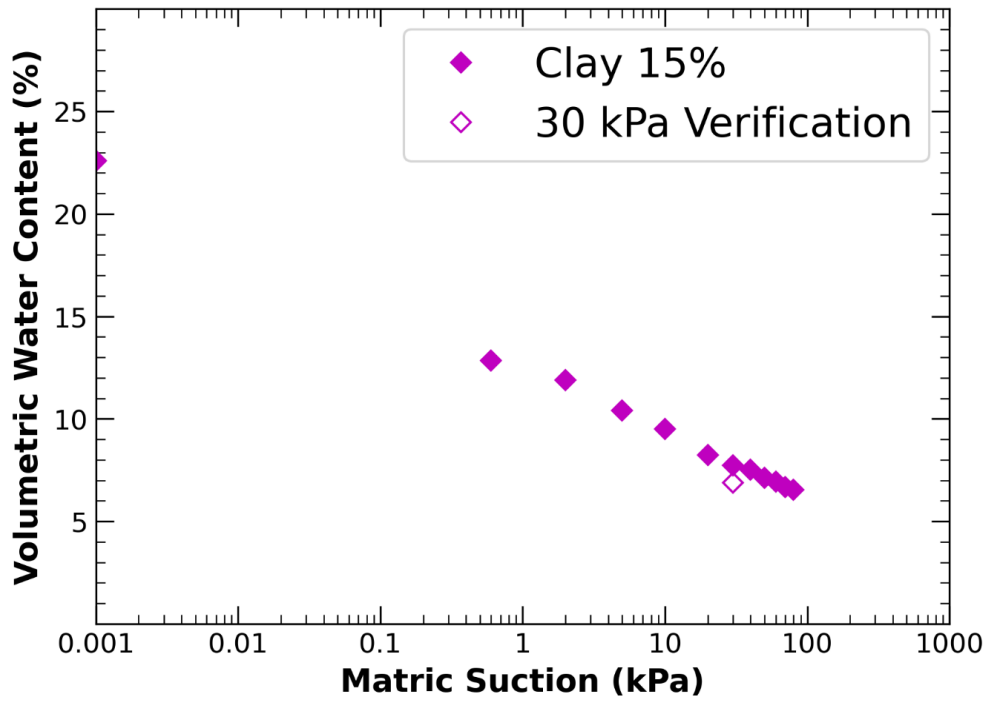
Figure A.10: Clay test with verification test

Appendix B
LSDS Testing Results

(a)

(b)

(c)

(d)
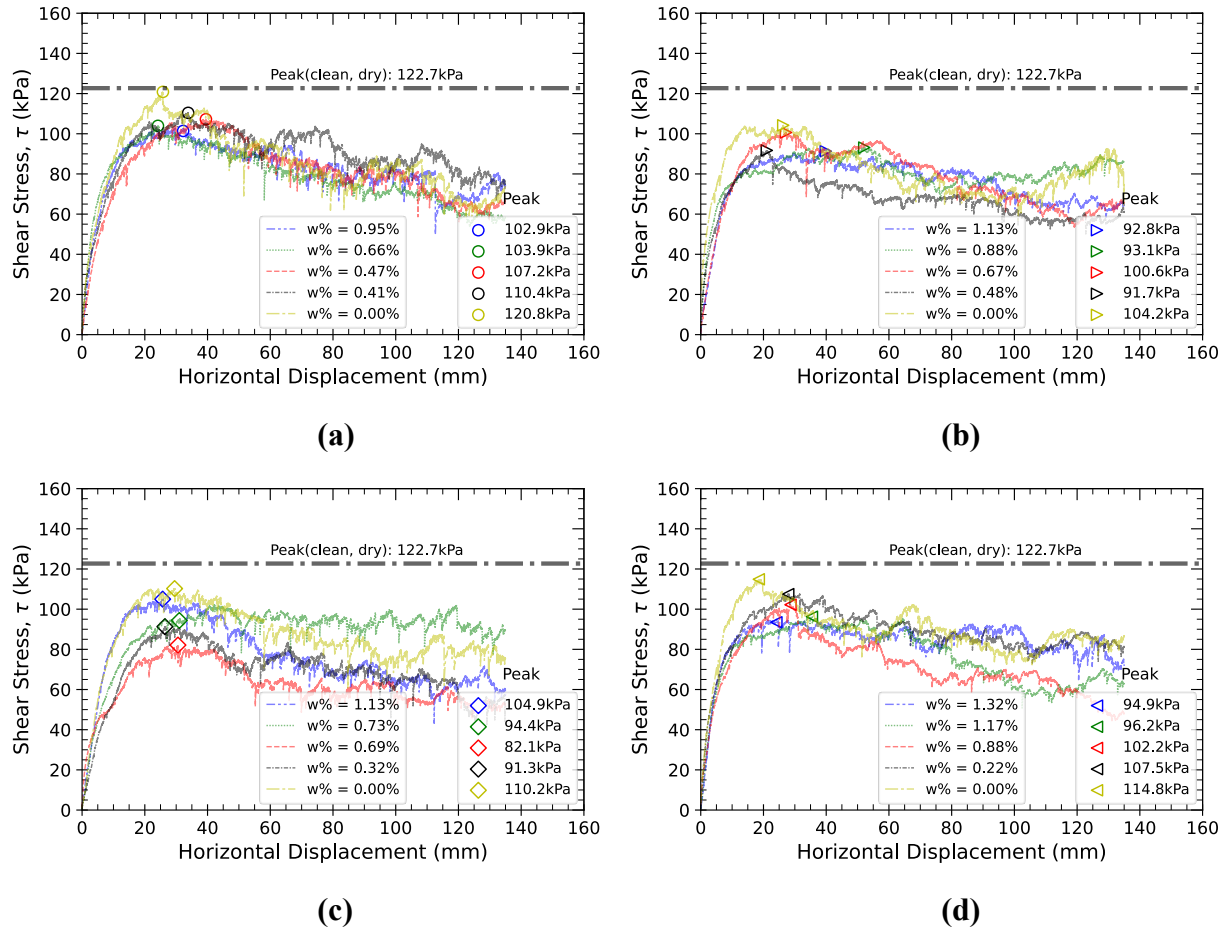
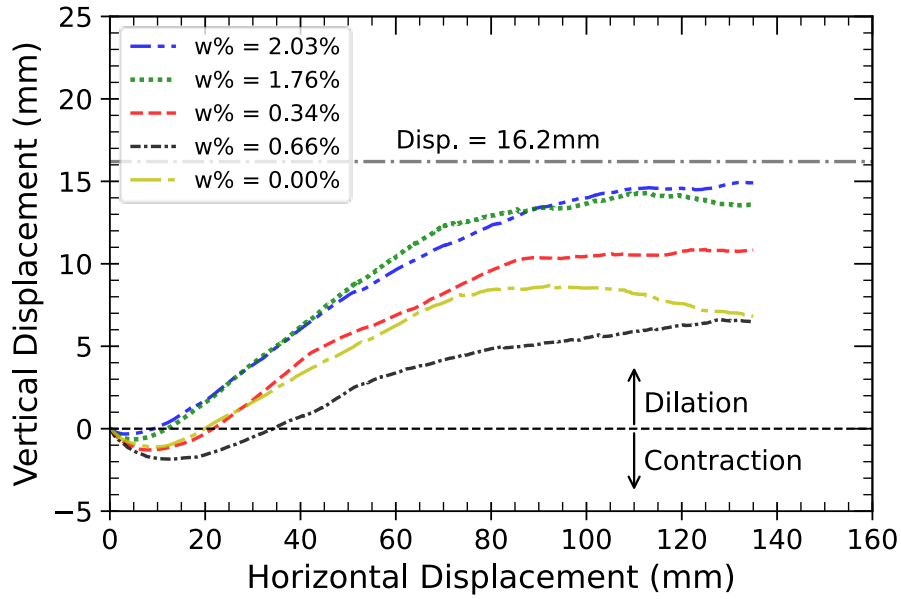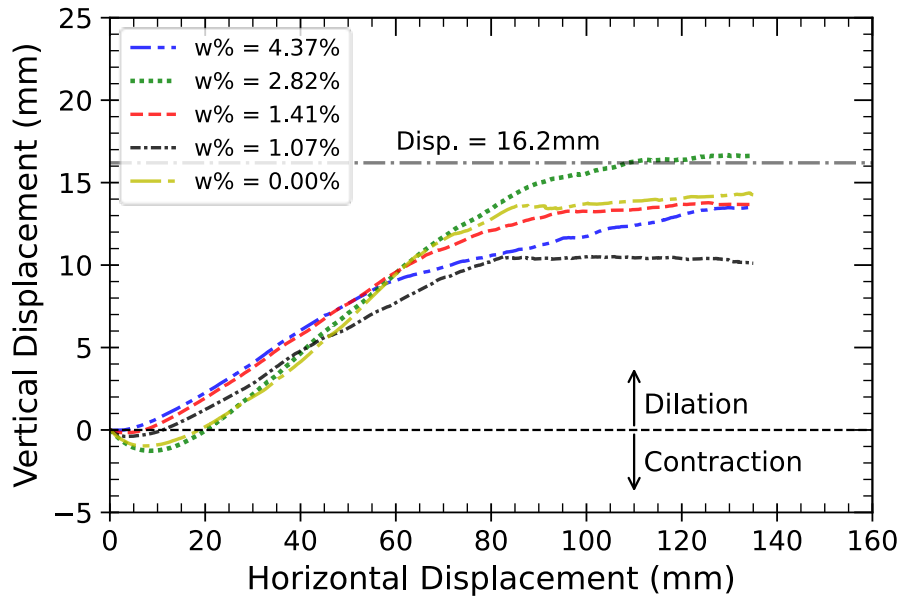**Figure B.1: Shear stress response as a function of horizontal displacement under different gravimetric water content conditions for (a) 5% Sand 1 (SP) fouled ballast; (b) 10% Sand 1 (SP) fouled ballast; (c) 10% Sand 2 (SP) fouled ballast; and (d) 15% Sand 2 (SP) fouled ballast**
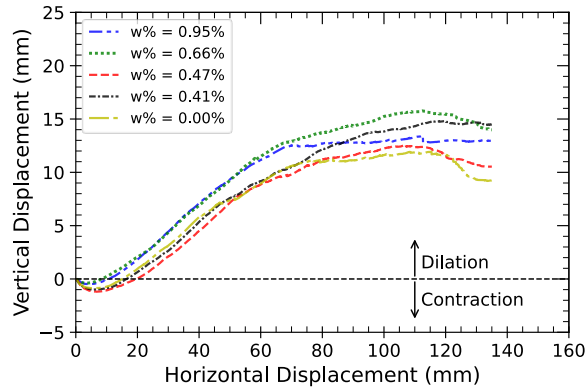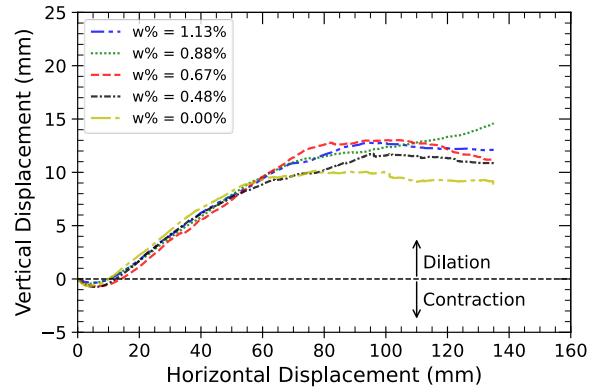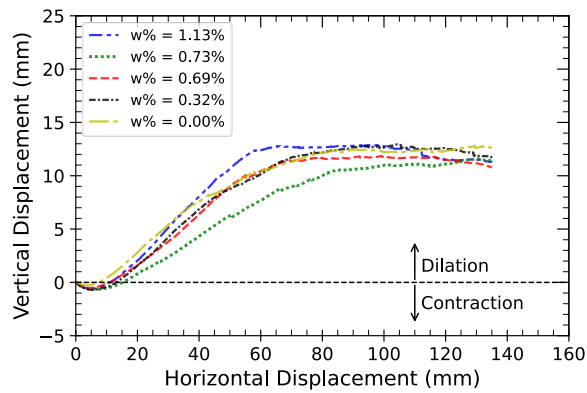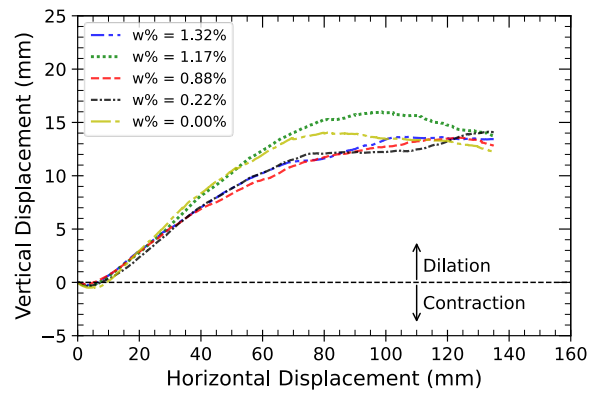
Figure B.2: Vertical versus horizontal displacement under different gravimetric water content conditions for (a) 5% Sand 1 (SP) fouled ballast; (b) 10% Sand 1 (SP) fouled ballast; (c) 10% Sand 2 (SP) fouled ballast; and (d) 15% Sand 2 (SP) fouled ballast
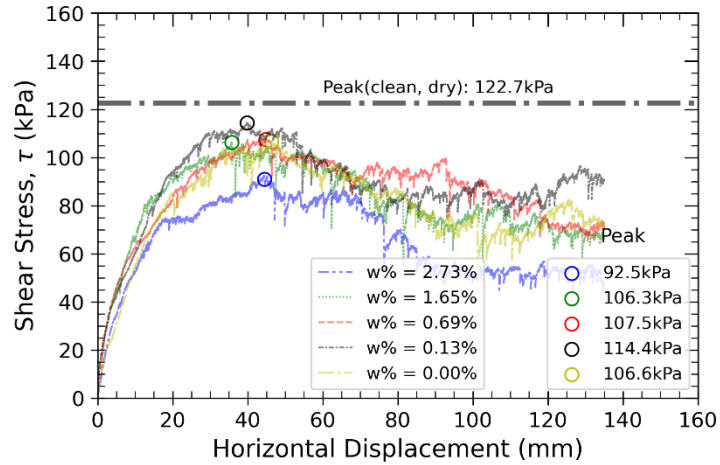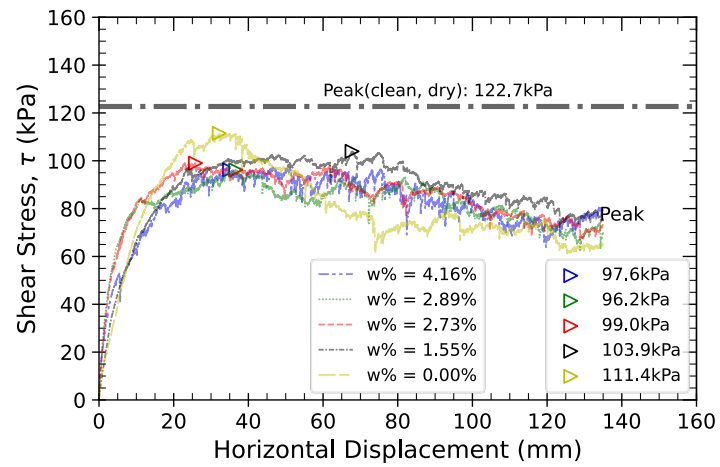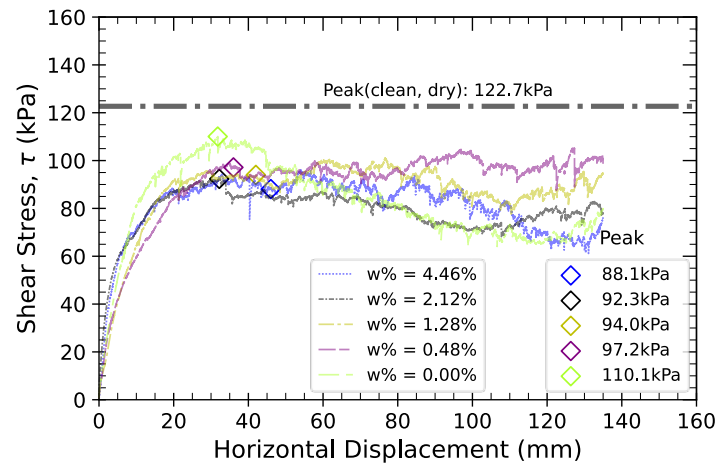
Figure B.3: Shear stress response as a function of horizontal displacement under different gravimetric water content conditions for (a) 5% Clay (CL) fouled ballast; (b) 10% Clay (CL) fouled ballast; and (c) 15% Clay (CL) fouled ballast
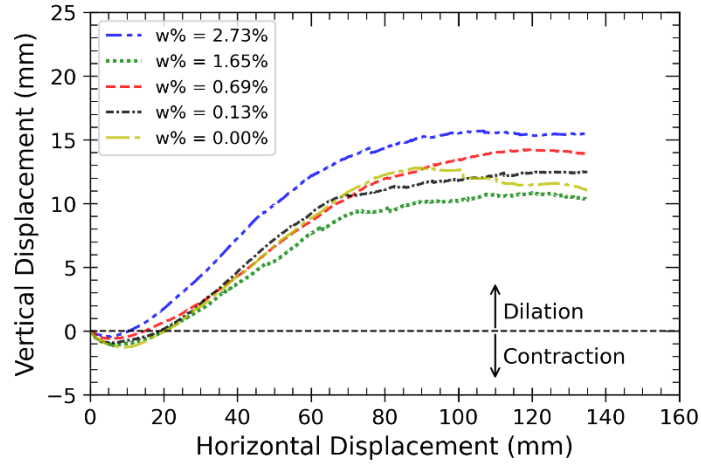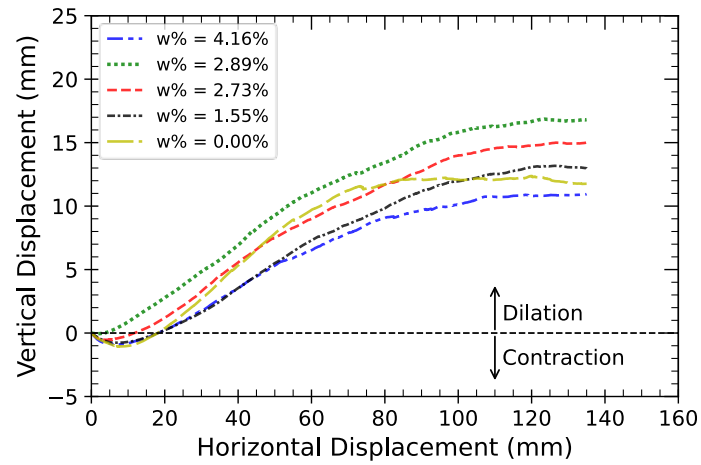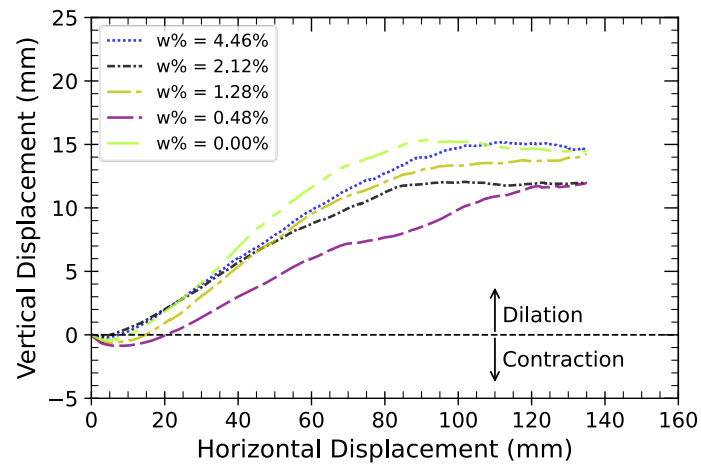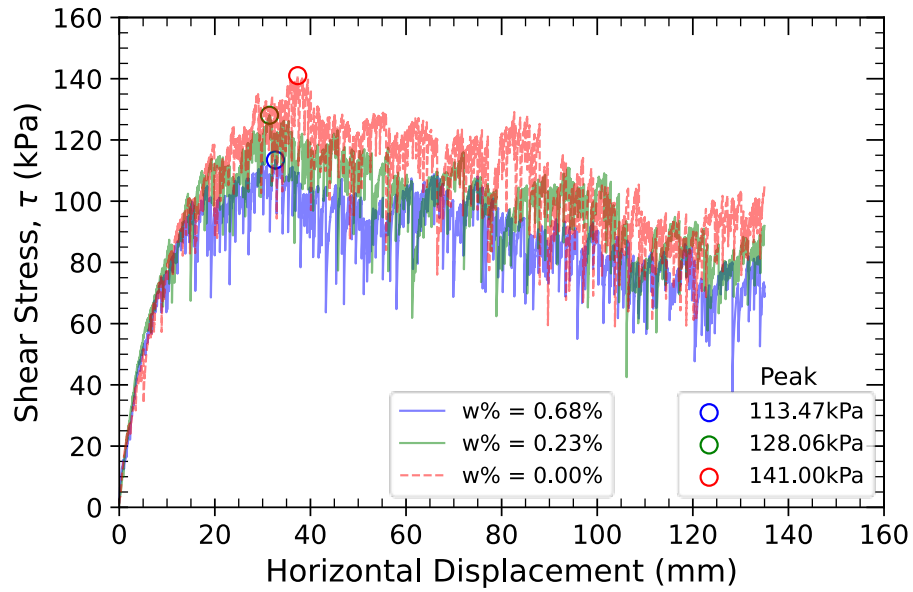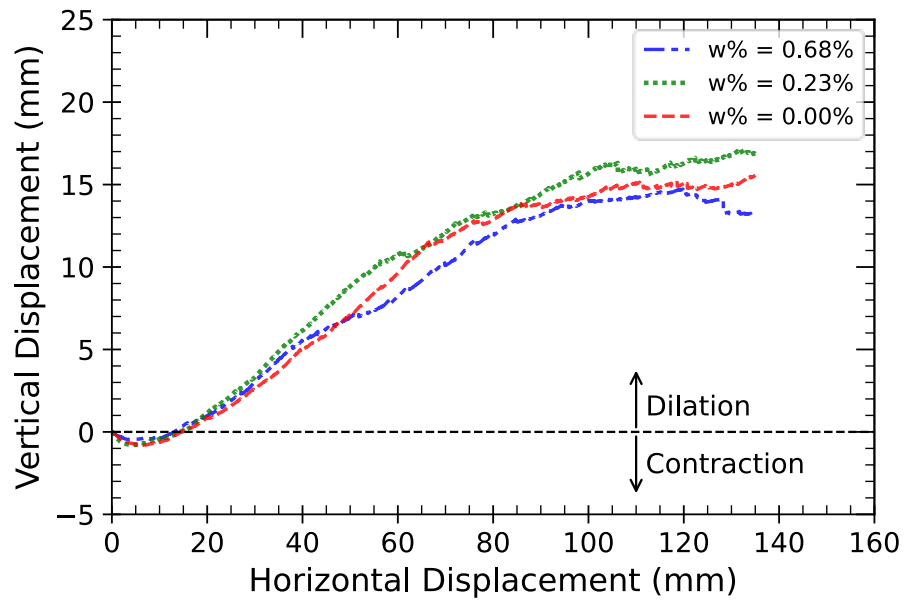
Figure B.4: Vertical versus horizontal displacement under different gravimetric water content conditions for (a) 5% Clay (CL) fouled ballast; (b) 10% Clay (CL) fouled ballast; and (c) 15% Clay (CL) fouled ballast
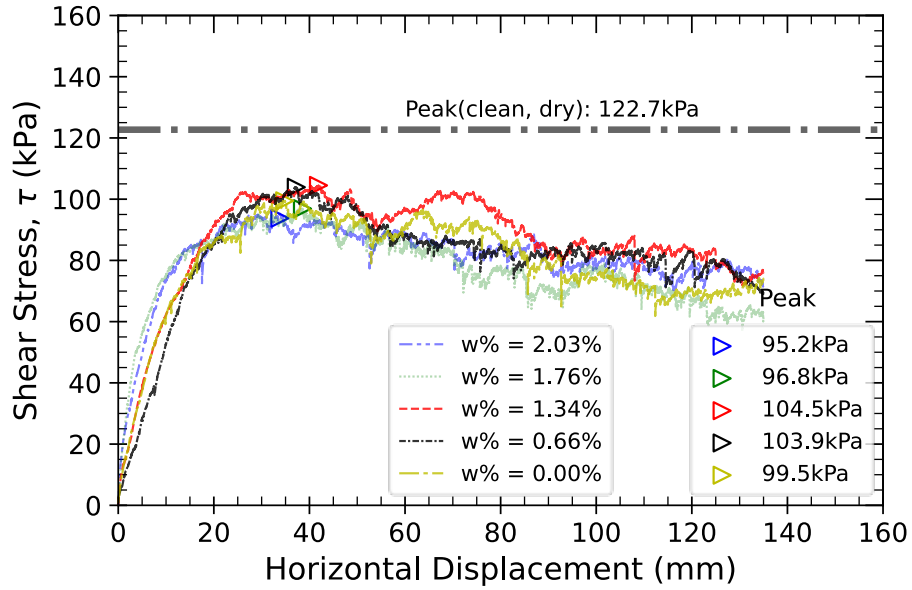
(a)
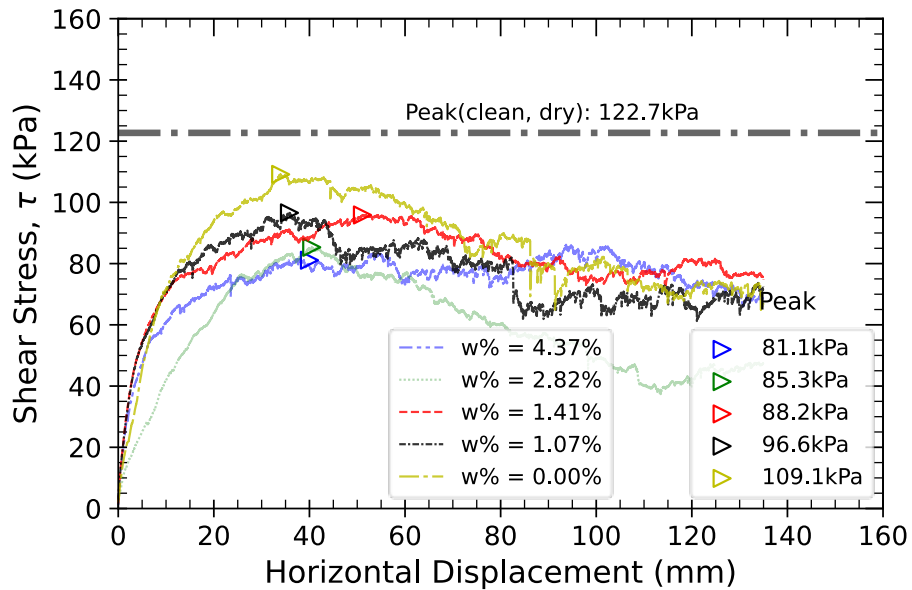
(b)

Figure B.5: **Shear stress response as a function of horizontal displacement under different gravimetric water content conditions for (a) 5% Coal (ML) fouled ballast; and (b) 10% Coal (ML) fouled ballast**

(a)

(b)

Figure B.6: Vertical versus horizontal displacement under different gravimetric water content conditions for (a) 5% Coal (ML) fouled ballast; and (b) 10% Coal (ML) fouled ballast

(a)

(b)

Figure B.7: (a) Shear stress versus horizontal displacement; and (b) vertical displacement versus horizontal displacement response under different gravimetric water content conditions for clean basalt

Appendix C
Complex Impedance Results

Table C.1: Summary of experimental setup tests

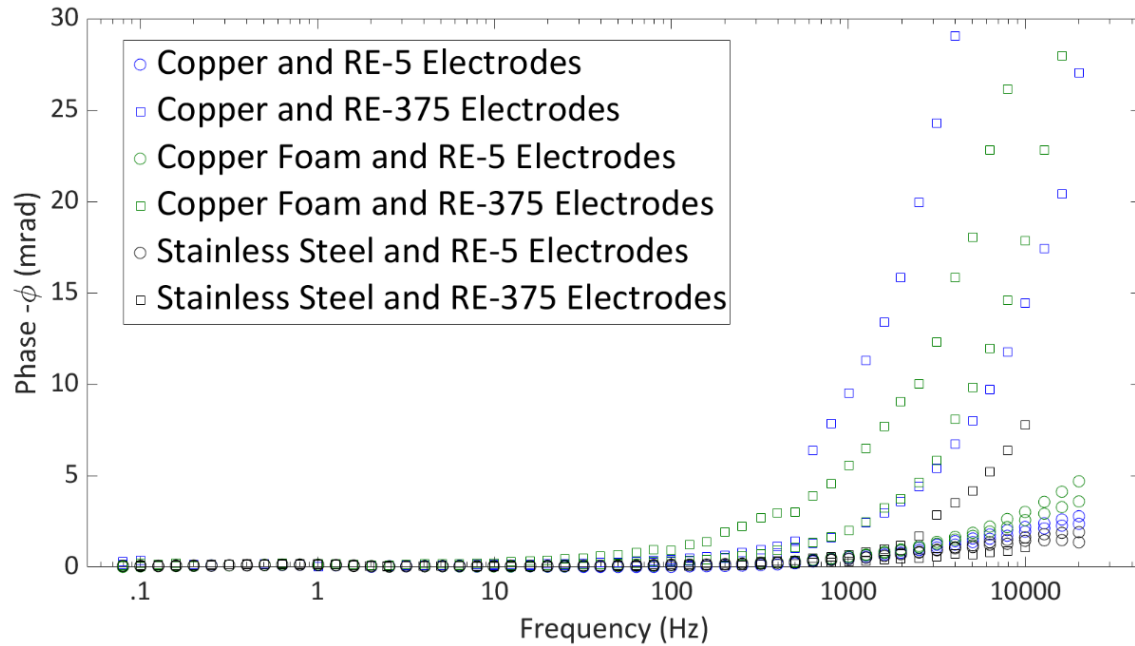| Control	Specimen	Experiment	Outcome
Current electrode material and potential electrode size	Fully saturated Ottawa sand	Curent electrode and potential electrode comparision	Fully saturated sand current electrodes yield similar results.
		Curent electrode comparision with RE-5 electrodes	RE-5 potential electrode preferred over RE-375.
		Curent electrode comparision with RE-375 electrodes	
	Fully saturated all ballast fouling specimens	Potential electrode comparision with copper electrodes.	RE-5 potential electrode preferred over RE-375
	Saturated vs unsaturated clay with chosen electrode	Curent electrode comparision with RE-5 electrodes	Negligible difference between copper and foam when unsaturated clay
	Validation	Final configuration validation with water test	Copper foam current electrodes and RE-5 potential electrodes
Minimum possible degree of saturation with copper foam electrodes	Sand 2, saturated to 15% saturation	Phase angle of Sand 2 from fully sautrated to 15% saturated with copper foam current electrodes and RE-5 potential electrodes	Results erradic below 20% saturation. If lower saturation needed, experimental setup should be modified
	Coal, saturated to 15% saturation	Phase angle of coal from fully sautrated to 15% saturated with copper foam current electrodes and RE-5 potential electrodes	Results erradic below 20% saturation. If lower saturation needed, experimental setup should be modified
	Clay, saturated to 15% saturation	Phase angle of clay from fully sautrated to 15% saturated with copper foam current electrodes and RE-5 potential electrodes	Lower degree of saturation possible with clay due to good contact with electrodes

Figure C.1: Current electrode and potential electrode comparison on fully saturated Ottawa sand specimens; the results from the smaller RE-375 electrodes were highly variable
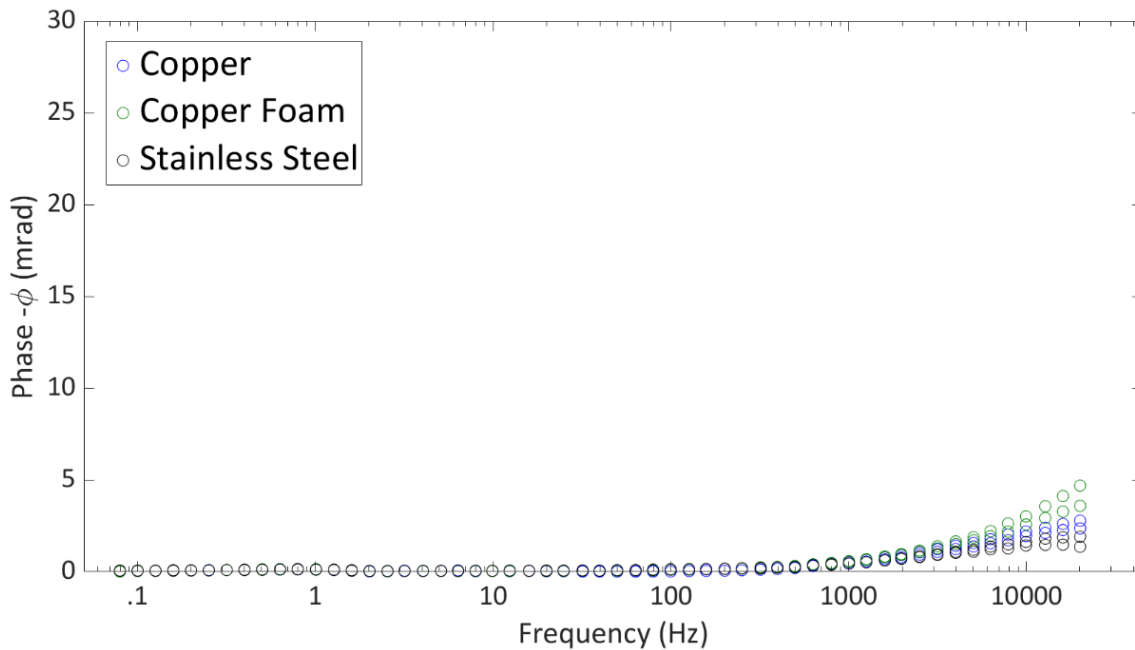

Figure C.2: Current electrode comparison on saturated Ottawa specimens with RE-5 electrodes; there was negligible difference in electrode material when using fully saturated specimens
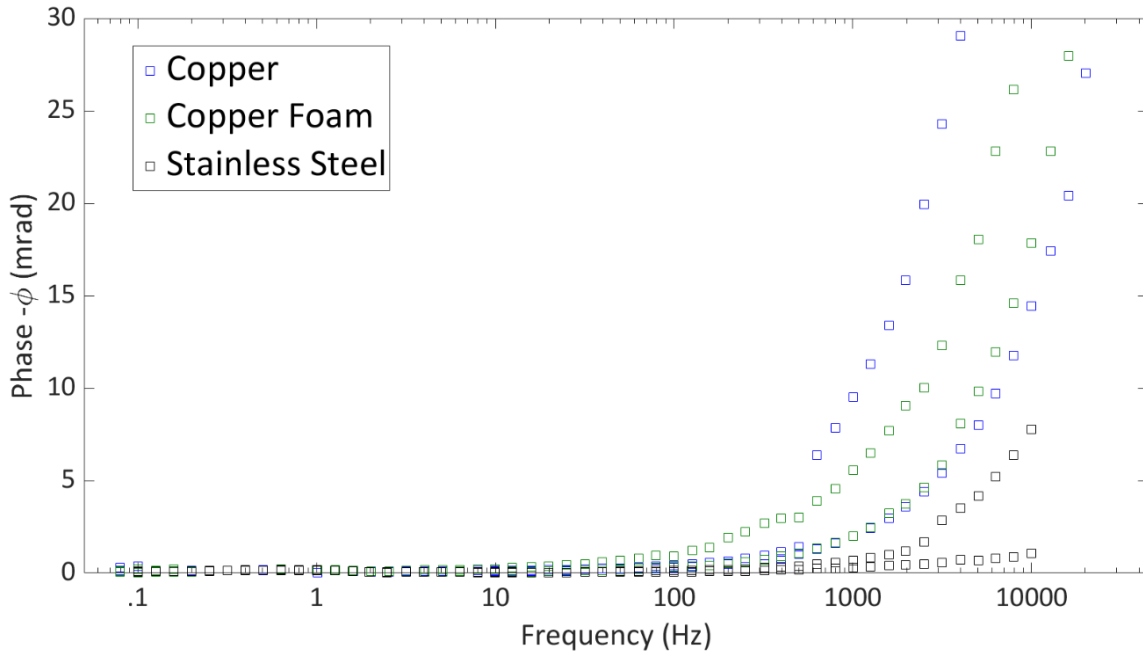
Figure C.3: Current electrode comparison on saturated Ottawa specimens with RE-375 electrodes; results were highly variable, despite fully saturated specimens
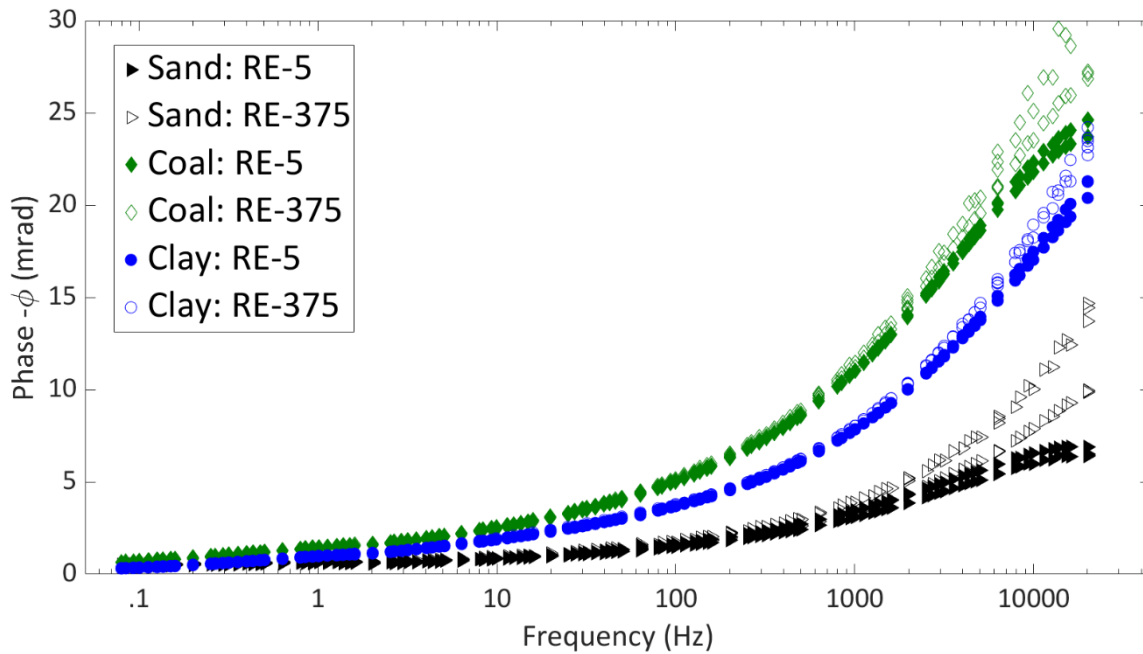

Figure C.4: Potential electrode comparison on saturated ballast fouling specimens with copper electrodes; most variability was noted in the sand where it was difficult to maintain contact with the RE-375 electrode and sand (Note that the response of the coal is highest because at this stage the density of the materials was not as shown in the main report)
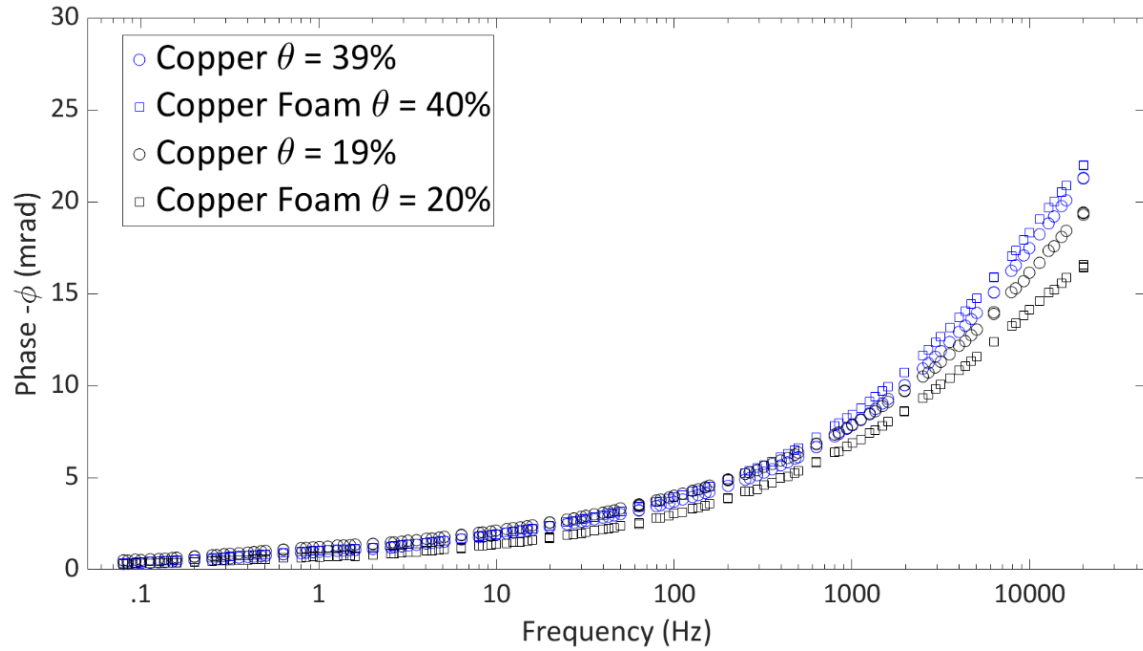
Figure C.5: Current electrode comparison (copper and copper foam) on saturated and unsaturated clay specimens with RE-5 electrodes
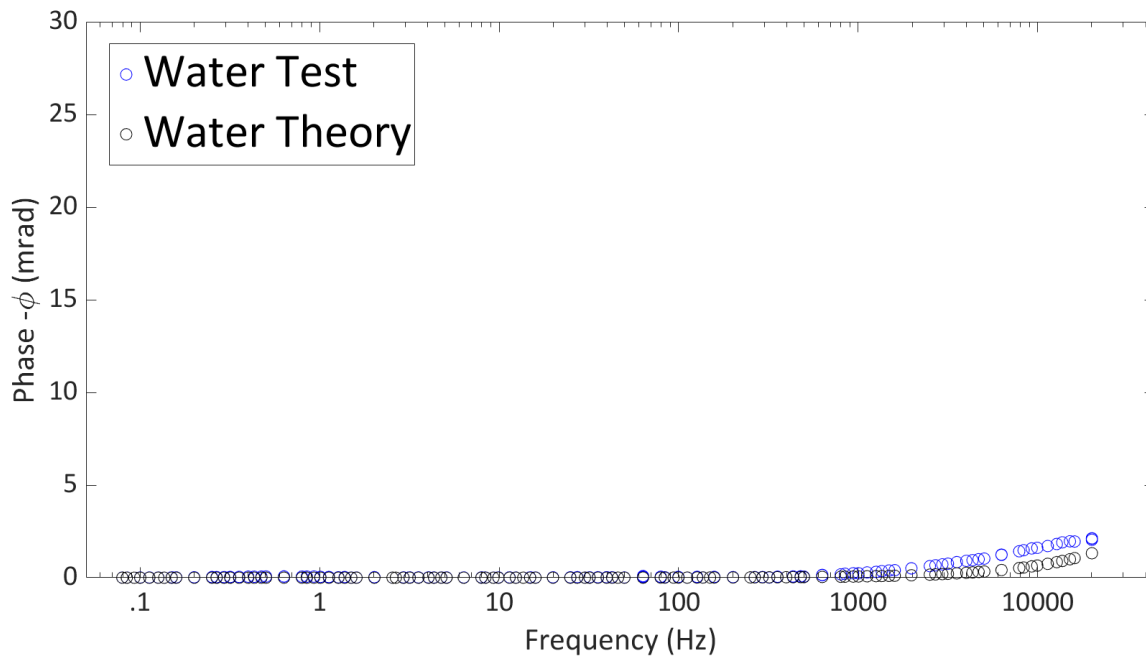

Figure C.6: Final configuration validation comparing a water test with water theory: Copper foam current electrodes and RE-5 potential electrodes
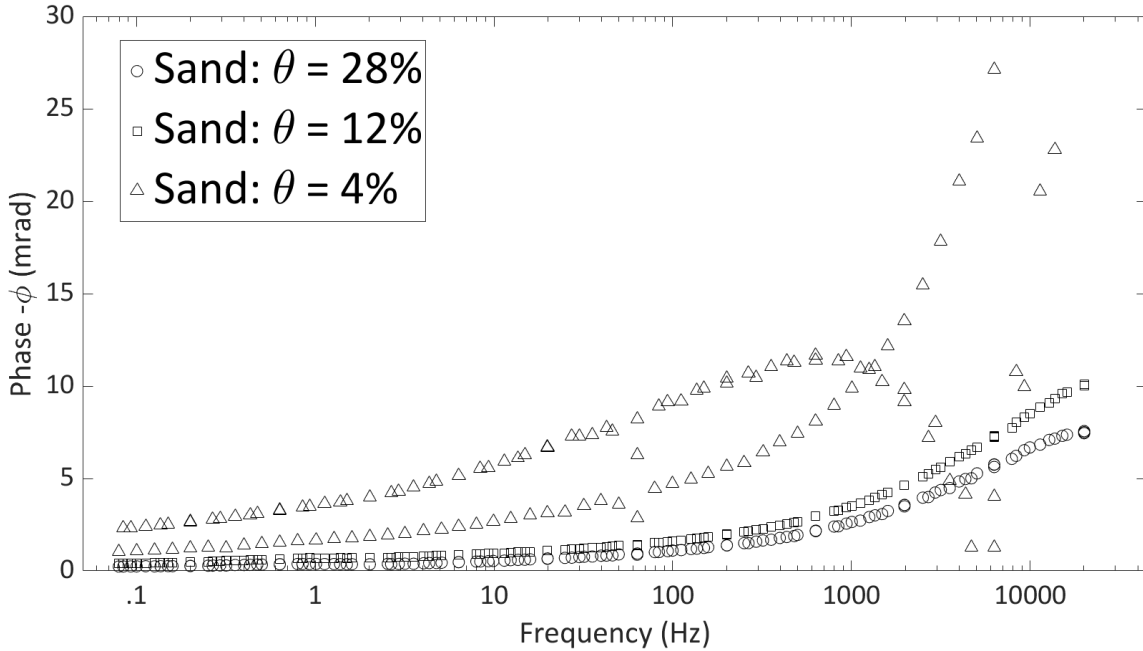
Figure C.7: Phase angle of Sand 2 from fully saturated to 16% saturated with copper foam current electrodes and RE-5 potential electrodes (The observed peak in the θ=4% specimens are likely due to poor contact due to the low degree of saturation and are considered noise)
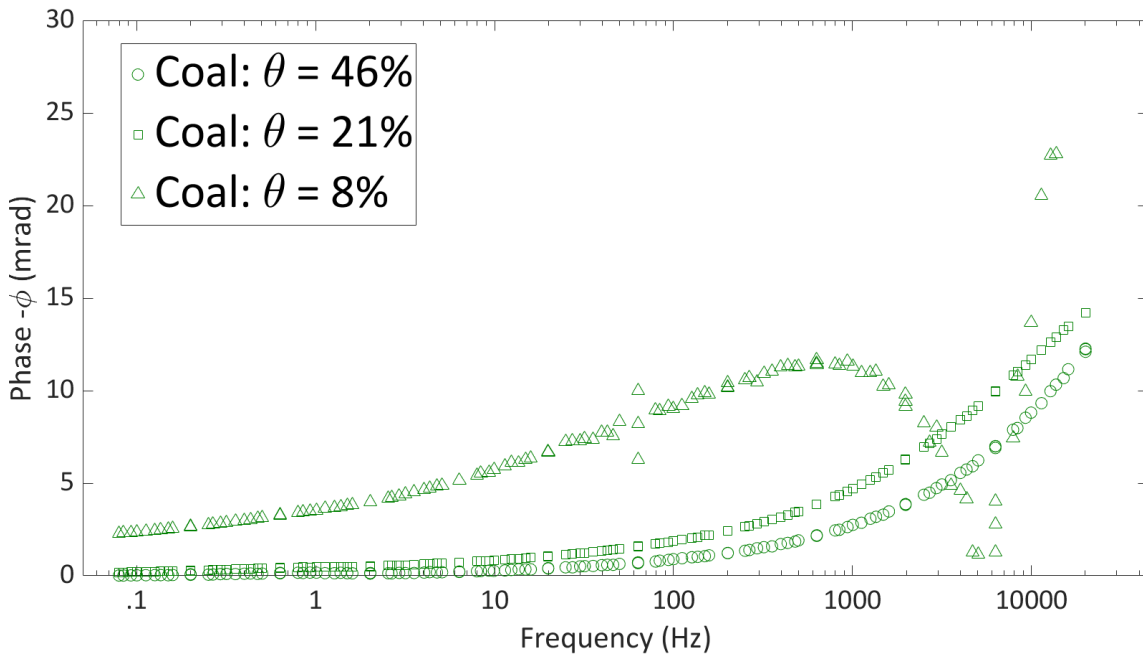

Figure C.8: Phase angle of coal from fully sautrated to 16% saturated with copper foam current electrodes and RE-5 potential electrodes (The observed peak in the θ=8% specimens are likely due to poor contact due to the low degree of saturation and are considered noise)
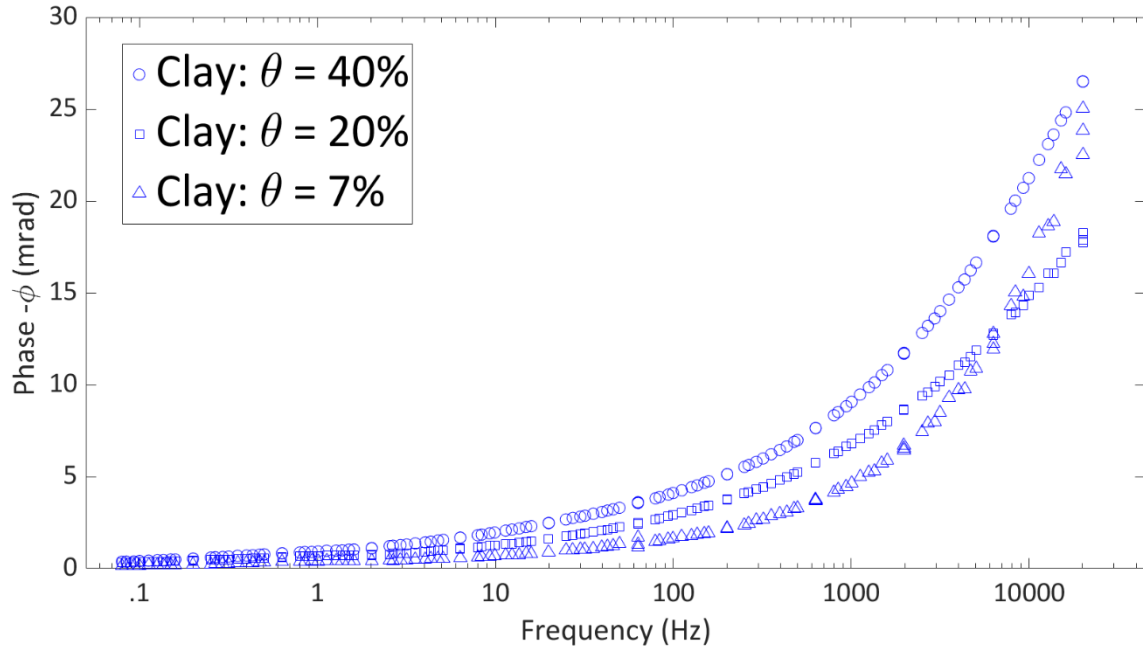
Figure C.9: Phase angle of clay from fully saturated to 15% saturated with copper foam current electrodes and RE-5 potential electrodes; there is no peak at the lowest degree of saturation due to good contact between the clay and the electrode compared to the other materials

Abbreviations and Acronyms

ACRONYM	DEFINITION
AREMA	American Railway Engineering and Maintenance-of-Way Association
ASTM	American Society for Testing and Materials
CL	Low plasticity clay, according to the USCS
FRA	Federal Railroad Administration
GPR	Ground Penetrating Radar
HAE	High Air Entry
LSDS	Large-Scale Direct Shear
ML	Low plasticity silty, according to the USCS
SC-SM	Silty, clayey sand, according to the USCS
SM	Silty sand, according to the USCS
SP	Poorly graded sand, according to the USCS
SW	Well graded sand, according to the USCS
SWCC	Suction Water Characteristic Curves
TRIM	Transient Water Release and Imbibition Method
USCS	Unified Soil Classification System